Scientific Journal of
University of Benghazi

Volume 38, Issue 2, (2025)

It deals with various branches of human, applied and medical knowledge

Publishes research in English

Guidelines for Submission

-Only articles originally written in English (NOT translated to English) are accepted for submission.

-The submission has not been previously published or being under consideration elsewhere.

-The submission file is in Microsoft Word format (.doc,.docx)

-The submitted articles should adhere to originality and publishing ethics.

-The similarity of the article should not exceed 20%.

-The submission should include a separate title page, the main article and the journal submission form.

-Article should have no more than 6 authors.

-The main article should be divided into; Title, Abstract, Keywords, Introduction,

-Material and Methods, Results and Discussion, Conclusion and References.

-The text is single-spaced, Times New Roman with a 12-point font.

-The text must not be more than 3000 words excluding abstracts and references.

-All figures and tables should be well presented, organized and consistent with the text.

-All figures must be prepared as (.tiff) or (.jpeg) format for the width of A4 size (6.27 in) with a minimum resolution of 300 dpi.

-The role of authors should be provided.

-Ethical approval when applicable should be provided.

-Any conflict of interest should be declared.

-Vancouver referencing style should be used.

-URLs/DOIs in the references list should be included where available.

Editorial Board

University of Benghazi Scientific Journal - University of Benghazi, Office No. 12, University of Benghazi - Al-Humaidah

Email: sjuob@uob.edu.ly **- Website:** http://journals.uob.edu.ly/sjuob

Editorial Board Members

Dr.Abdelhamid Elbarasi

Dr. Mohamed A. E. Abdalla

(Applied Sciences)

Porf.Dr.Daefalla M. Tawati

Porf. Dr.Mayeen Uddin Khandaker

(Applied Sciences)

Dr.Allaaeddin A. El Salabi

(Medical Sciences)

Dr. Ahmad S. Emrage

(Humanities)

Editorial Board Members

Dr. Abdelhakim M. Elbarsha

(Medical Sciences)

Rwaida Aljadi

(Technical Coordinator)

Khalifa A. Al-Athram

(Administrative Coordinator)

University of Benghazi Scientific Journal - University of Benghazi, Office No. 12, University of Benghazi - Al-Humaidah

Email: *sjuob@uob.edu.ly* **- Website:** *http://journals.uob.edu.ly/sjuob*

Preface

The Second Issue of Volume 38, 2025

The Scientific Journal of the University of Benghazi is pleased to announce the publication of its thirty-eighth issue, second edition, for December 2025.

This issue contains twelve research papers in the humanities, applied sciences, and medical sciences.

The published papers have undergone the journal's established procedures, including plagiarism screening, artificial intelligence detection, and scientific peer review by distinguished reviewers from Libyan and Arab universities.

The Editor-in-Chief extends his gratitude to the members of the Editorial Board for their efforts in serving scientific research and enhancing the university's standing, and encourages researchers to continue publishing in the journal in forthcoming issues.

Sincerely

The Editor-in-Chief and Editorial Board

The Scientific Journal of University of Benghazi (SJUOB)

Table of Contents for Volume 38 Issue 2

Scientific Journal of University of Benghazi (2025)

Humanties

Scientific Journal of University of Benghazi

SJUOB (2025) 38 (2) Humanities Sciences: Hadaga & Elfalfal, 10 – 22
www.sjuob.uob.edu.ly

Libyan EFL Teachers' Perceptions of AI Integration in English Teaching: A Case Study at Benghazi University.

Hana Mahmoud Hadaga[1]*, Amal Mohammed Elfalfal[1].

1 Department of English, Faculty of Languages, University of Benghazi.

DOI: 10.37376/sjuob.v38i2 | Received:21/07/2025 | Accepted:17/10/2025 | Publishing: 23/12/2025

ABSTRACT

There is an inevitability and increasing use of technologies such as Artificial Intelligence (AI) in language teaching and learning. This research investigates EFL Libyan teachers' perceptions of the effectiveness of integrating AI tools in EFL teaching in the Libyan context. The study employed a quantitative approach of research in which a questionnaire was distributed to collect data from 20 EFL Libyan teachers in the department of applied linguistics at the Faculty of Languages at Benghazi University in Libya. The questionnaire examined data relevant to Libyan EFL teachers' perspectives on integrating AI in their teaching process and the challenges encountered. The results showed that most participants had a positive attitude towards using AI in their teaching. The majority believed that AI is important for helping students improve their language skills and making English teaching more effective. In addition, they mutually agreed that AI encouraged their students to participate more actively in class and helped to reduce their anxiety about making mistakes. However, the study revealed that participants collectively faced challenges in using AI. One major challenge was that they mostly relied on self-study to learn about these technologies rather than formal training. Findings of this study provide feedback to the head dean of the Department of Applied Linguistics for possible improvements. Furthermore, these findings can inform future enhancement initiatives in other similar Libyan EFL contexts. A better integration of AI into educational settings is needed, and more support and training are necessary for successful implementation.

KEYWORDS: Instructors, EFL context, Artificial Intelligence.

*Corresponding Author: Hana Mahmoud Hadaga, hana.hadaga@uob.edu.ly

 ISSN: Online 2790-1637, Print 2790-1629
National Library of Libya, Legal number: 154/2018

1.INTRODUCTION

In recent years, there has been a notable integration of technology, particularly artificial intelligence (AI) within EFL classrooms. AI tools, such as chatbots, voice recognition systems, and platforms like ChatGPT, have demonstrated effectiveness in enhancing the teaching and learning of English [1, 2]. The proliferation of mobile computing and widespread internet access has catalyzed the development of online learning platforms providing learners with convenient access to diverse educational resources [3, 4, 5].

The term "artificial intelligence" (AI) was first coined by John McCarthy who was the inaugural professor of AI at Stanford University in 1955. He defined AI as the science and engineering of crafting intelligent machines [6]. AI fundamentally involves the creation of computer systems or machines that demonstrate a range of competencies such as computer vision, speech recognition, and problem-solving [7].

Many researchers (Chen et al., Tang et al., and Zhai et al.) believe that AI can greatly improve language education by enhancing teaching methods and helping students achieve better results [8, 9, 10]. Some think that AI can reduce teachers' workload by handling repetitive tasks like grading and giving feedback. This allows teachers to spend more time on direct teaching and supporting students [11]. Others (Like Jeon [12]) believe that AI helps students develop decision-making skills and prediction abilities [12]. Various AI tools can assist learners in improving their language skills [2, 13]. A significant benefit of incorporating AI into EFL classrooms is its ability to personalize learning providing individualized feedback [14, 2].

Despite recognizing the above benefits of AI tools, many educators expressed concerns about their impact on academic learning. Some argued that using AI may negatively affect the quality of education and students' learning outcomes [15]. Students might misuse AI technologies for dishonest purposes such as, plagiarism which could affect the authenticity of their work [16]. Another major concern of AI tools in learning is that students might use generative AI tools to cheat in their written assignments, presentations, and exams [17]. This could weaken students' writing skills and critical thinking, as they depend more on automated technologies to complete their work [18]. Additionally, some educators stress the importance of human interaction in language learning, especially for understanding cultural nuances and context, which AI cannot fully provide [19, 20]. Moreover, incorporating AI into EFL classrooms comes with challenges including the costs and technical skills needed to establish and maintain these systems [21].

The extent of application of AI in EFL contexts has been recognized many by researchers. For example, Alshumaimeri and Alshememry [22], in 2024, conducted a systematic review of the literature on the applications of AI in English as a Foreign Language (EFL) education. Findings suggested that argumentative writing in AI applications had received the most research attention, followed by language education, automated feedback, surveys, and translation research [22]. Also, Abolkasim and Hasan [23] evaluated the potential for incorporating Artificial Intelligence (AI) technologies in the process of learning at the university level in Libya, examining both the students' and staff members' perspectives. The results showed that there was a strong tendency to use ChatGPT in the educational system in Libya by both the students and instructors, for purposes such as scientific research, studying, planning lectures, answering assignments, and writing tasks. However, some concerns were raised about students becoming too dependent on AI tools, which could affect their integrity and creativity [23]. Furthermore, Hmouma [24] conducted a study in 2024 where views of EFL students from Al-Rifaq University in Tripoli/ Libya regarding the use of AI-based language learning applications were examined. The results showed that most participants were in favor of using AI tools, and expressed a preference for

 ISSN: Online 2790-1637, Print 2790-1629
National Library of Libya, Legal number: 154/2018

personalized learning experiences and the immediate feedback that AI provides. However, there were notable concerns about the possibility of AI replacing teachers in the future [24].

Although AI is becoming more common in education [25], its exact role is still unclear [26], making it difficult for teachers to understand how best to use it in EFL classrooms. Moreover, there is still a need for more understanding of educators' perception of AI tools in teaching and learning [23]. The significance of this research lies in the fact that, to the best of the researcher's knowledge, no previous study has investigated the perceptions of EFL teachers in the Department of Applied Linguistics at the Faculty of Languages in Benghazi towards the use of AI tools in teaching. Therefore, this study aimed to add to the literature and to gain insights into the perceptions of EFL Libyan instructors regarding the benefits and challenges of integrating AI in Libyan EFL classrooms. This research would assess the advantages and obstacles associated with using AI applications in EFL classes, aiming to provide valuable insights and recommendations for the head dean of the Faculty of Languages. Specifically, the study aimed to answer the following question:

1.What perspectives do Libyan EFL instructors in the department of Applied Linguistics at the Faculty of Languages at Benghazi University in Libya hold regarding the use of using AI tools in teaching English as a Foreign language in Libyan EFL classrooms?

2. MATERIALS AND METHODS

The researcher, being a member of the Applied Linguistics Department, chose her colleagues to take part in the study because she is directly involved in this teaching environment. The main goal of selecting this group was to understand their views on using AI tools in teaching aiming to show the overall situation among the department's teachers and to offer feedback to the head dean for potential improvements. A total of 20 Libyan EFL instructors from the Department of Applied Linguistics at the Faculty of Languages, Benghazi University, took part. These participants included both male and female teachers and represented the whole population of the teaching staff of the department for the academic year 2024/2025. The head dean of the Faculty of Languages confirmed this selection.

This study used a descriptive-analytical approach. A quantitative research method was employed due to its efficiency in terms of time as it allows the collection of data from a significant number of participants within a relatively short period. Moreover, this method facilitates objective analysis and interpretation through the use of numerical data and statistical tools [27]. A closed-ended questionnaire was employed based on Kumar [27] who noted that the use of closed-ended questions in a questionnaire facilitates the collection of the desired data by the researcher and simplifies the analysis process.

The selected questionnaire was employed because it provided relevant data to this research questions mentioned earlier. That is, the questionnaire focused on two main topics: (1) the role of AI in learning English as a second Language, and (2) how utilizing AI can improve the English Language Teaching (ELT) process, with the second topic focusing on the challenges that are associated with the application of AI to the educational process. The questionnaire included seven items. Each item used a Likert scale from one to five. The five possible responses were: strongly agree, agree, neutral, disagree, and strongly disagree. The questionnaire was adopted from Alhalangy and AbdAlgane [19]. And it was distributed to participants in person not online.

3. RESULTS AND DISCUSSION

To analyze the data collected from the questionnaire responses, the researcher employed the formula provided by Zamri et al. [28], which was as follows:

$$P = \frac{F}{N} \times 100\%$$

Where, P= Percentage, F= Frequency, N= Total number of the respondents. The total responses for each

 ISSN: Online 2790-1637, Print 2790-1629
National Library of Libya, Legal number: 154/2018

item should add up to 100%. After applying this formula to the participants' responses, the results were described statistically. These findings are presented in Table (1) below.

Table (1): Descriptive Statistics of Participants' Responses to the Questionnaire Items

Questionnaire Statement	Strongly Agree	Agree	Neutral	Disagree	Strongly Disagree
1. Artificial Intelligence (AI) plays a significant role in promoting EFL learners' language skills.	65%	35%	0%	0%	0%
2. Utilizing AI could facilitate the ELT process.	60%	30%	5%	5%	0%
3. Integrating AI tools into ELT poses challenges for both instructors and learners.	10%	45%	40%	5%	0%
4. My professional development in using computer and internet services is based on self-training.	70%	20%	5%	5%	0%
5.I believe that incorporating AI into the classroom encourages learners to take an active role in their learning.	50%	30%	10%	10%	0%
6. AI technology reduces the stress of trial and error in learning.	30%	45%	5%	10%	10%
7. AI could cause boredom and a lack of desire to learn and teach EFL since both learners and teachers deal with machines.	10%	5%	30%	35%	20%

To ensure clear and smooth discussion to the questionnaire results presented in Table 1 above, the data from each item were presented using pie charts. These charts employed a distinct color scheme to represent the different Likert scale responses: blue for "strongly agree," green for "agree," yellow for "neutral," orange for "disagree," and red for "strongly disagree." This color-coding was chosen to visually separate the response categories, making the data easier to interpret and understand.

In the first item of the questionnaire, 65% of participants strongly agreed that AI plays a significant role in enhancing EFL learners' language skills, 35% had agreed as well. The results are illustrated in Figure 1 below.

 ISSN: Online 2790-1637, Print 2790-1629
National Library of Libya, Legal number: 154/2018

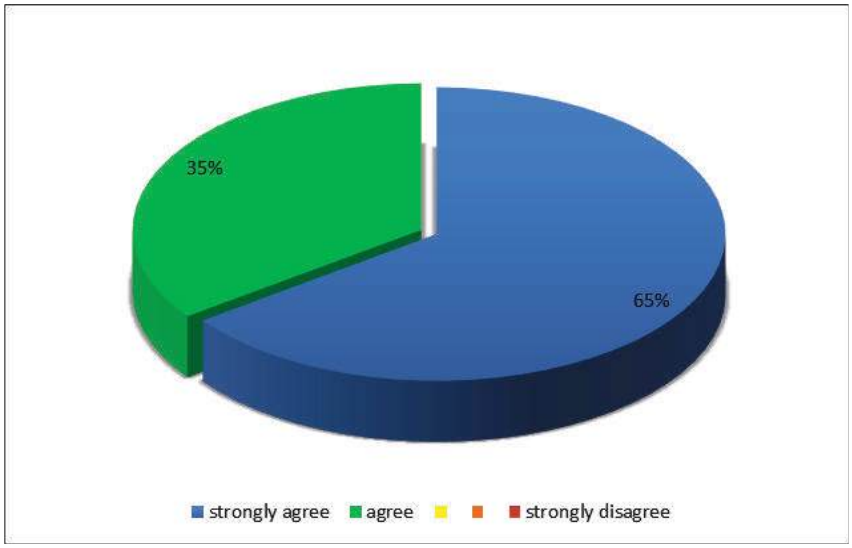

Figure 1: (Participants' Responses to the First Questionnaire Item).

The pie chart shows that all participants believe AI can enhance students' language skills, with 65% strongly agreeing (blue) and 35% agreeing (green). This positive perception may stem from teachers' experiences using AI in their classrooms, where it provided clear, easy-to-understand materials that helped learners practice effectively. Notably, no participants selected neutral, disagree, or strongly disagree options, indicating unanimous agreement with the statement.

In the second item of the questionnaire, participants were asked whether AI could help improve the process of teaching English as a foreign language (EFL). The results are illustrated in the pie chart below.

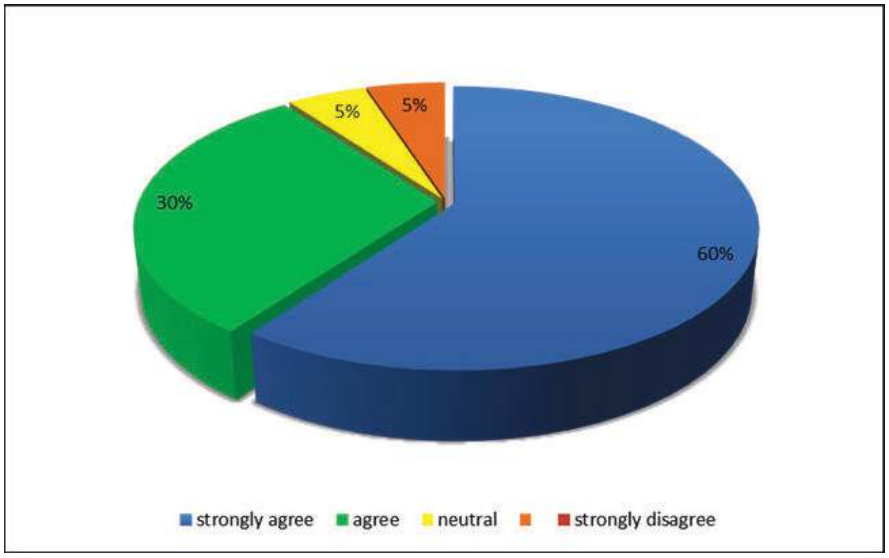

Figure 2: (Participants' Responses to the Second Questionnaire Item).

Figure 2 shows that most participants (60% strongly agreed (blue) and 30% agreed (green) have a positive attitude toward using AI to support English Language Teaching (ELT). This positive view may come from their own teaching experiences, where they used AI tools and saw how these tools made teaching easier and more effective. However, one participant (5%) gave a neutral response (yellow), and another participant (5%) disagreed (orange) with the statement about AI's usefulness. These less positive views may be due to concerns about AI's accuracy, with some fearing that AI might provide incorrect or misleading information. Additionally, they may believe that teaching is a personal and human activity.

In the third item of the questionnaire, participants were asked whether integrating AI tools into English Language Teaching (ELT) creates challenges for both instructors and learners. The results are shown in Figure 3 below.

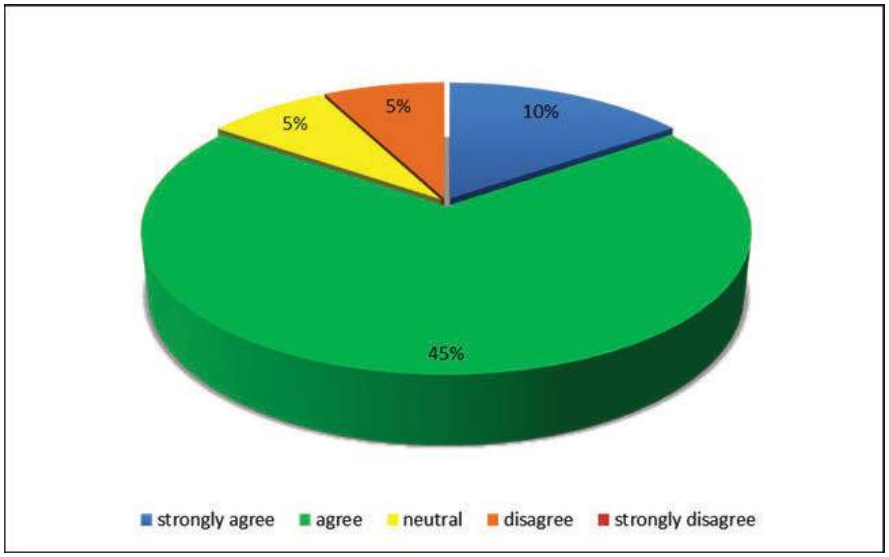

Figure 3: (Participants' Responses to the Third Questionnaire Item).

Figure 3 shows that more than half of the participants (45% in green and 10% in blue) agree that AI presents challenges for teachers and learners. This indicates that these participants likely have experienced using AI in their classrooms and understood the difficulties it could cause. It appears that they have directly encountered these challenges during their teaching. On the other hand, 5% of participants were neutral (yellow), and another 5% disagreed (orange). This may be because they have not yet used AI in their teaching or do not have enough knowledge about these challenges to fully recognize the problems involved.

Additionally, item four in the questionnaire explores whether participants' professional development in using computers and internet services stems from self-training. These results are illustrated in the pie chart below.

 ISSN: Online 2790-1637, Print 2790-1629
National Library of Libya, Legal number: 154/2018

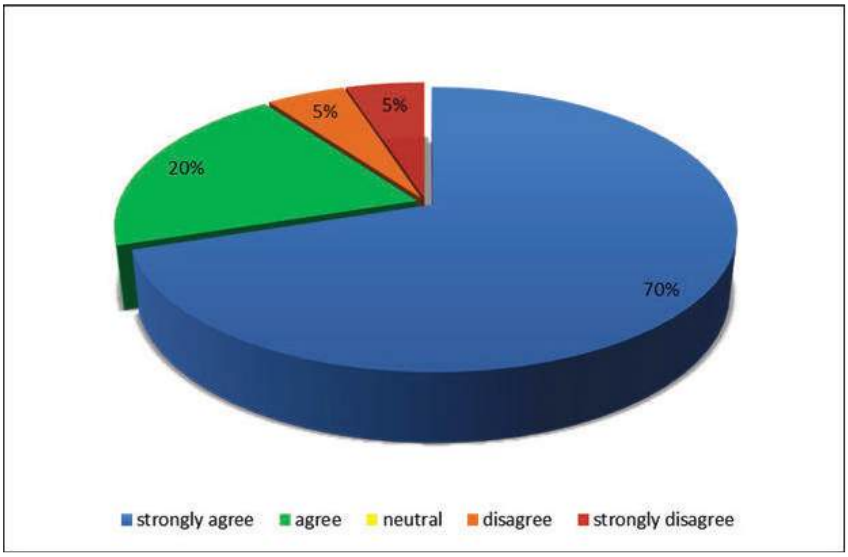

Figure 4: (Participants' Responses to the Fourth Questionnaire Item).

Figure 4 shows that most participants (70% in blue and 20% in green) agreed that their professional development in using computers and the internet is mainly based on self-training. This suggests that they have recognized the importance of improving their computer and internet skills and have seen their profession in teaching is a self-directed responsibility. However, 5% of participants disagreed, and another 5% strongly disagreed (shown in orange and red respectively). This disagreement might be because these participants rely more on formal training programs, such as workshops, seminars, or official sessions provided by their institutions.

Item five in the questionnaire asked participants whether using AI in classroom activities can help learners become more active in their learning. The results are clearly displayed in the pie chart below.

 ISSN: Online 2790-1637, Print 2790-1629
National Library of Libya, Legal number: 154/2018

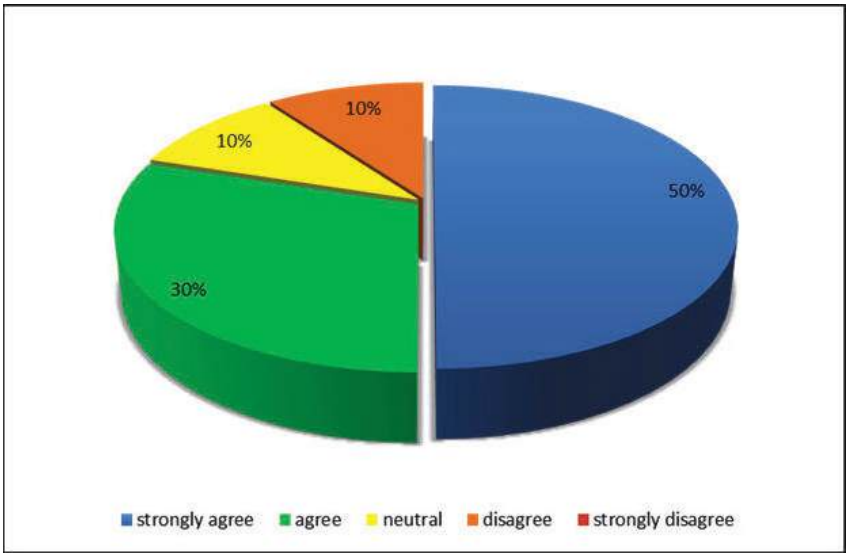

Figure 5: (Participants' Responses to the Fifth Questionnaire Item).

As indicated in Figure 5 above, most participants (50% strongly agreed in blue and 30% agreed in green) support the statement that using AI activities in the classroom helps students become more active learners. They likely hold this view because they have observed increased student participation when AI was used in their classes. 10% of participants were neutral (presented in yellow), possibly because they have not noticed any effects of AI or have not used AI in their teaching. Another 10% disagreed (reflected in orange), and none strongly disagreed. These participants may not rely on AI to engage their students or to select classroom activities that encourage their students' responsibility. This suggests that while many see AI as helpful for student engagement, some remain uncertain or skeptical about its role in the classroom.

Item six in the questionnaire investigates whether using AI technology reduces the stress caused by trial and error in learning. Results are clearly shown in the pie chart below.

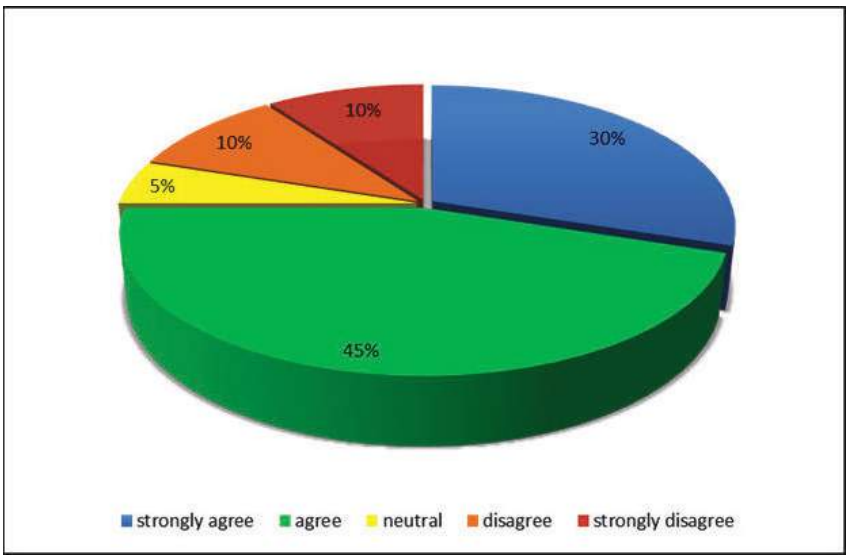

Figure 6: (Participants' Responses to the Sixth Questionnaire Item).

The figure above clearly indicates that most participants (30% strongly agreed in blue and 45% agreed in green) believe that AI tools can reduce stress by offering personalized learning and helping students handle difficult tasks more easily. This positive view may come from their experience using AI in classrooms, where it improved learning and reduced frustration. They also agreed that AI can provide emotional support and simplify complex tasks, which helps lower stress during learning. Five percent of participants were neutral about this statement. However, 10% strongly disagreed and another 10% disagreed. These participants might think that AI tools cause confusion and cognitive overload instead of making learning easier.

They may also believe that students benefit more from face-to-face explanations than from AI-based learning.

The seventh item in the questionnaire asked participants whether using AI could cause boredom and reduce motivation to learn and teach English as a Foreign Language (EFL). The percentages are shown in the pie chart below.

 ISSN: Online 2790-1637, Print 2790-1629
National Library of Libya, Legal number: 154/2018

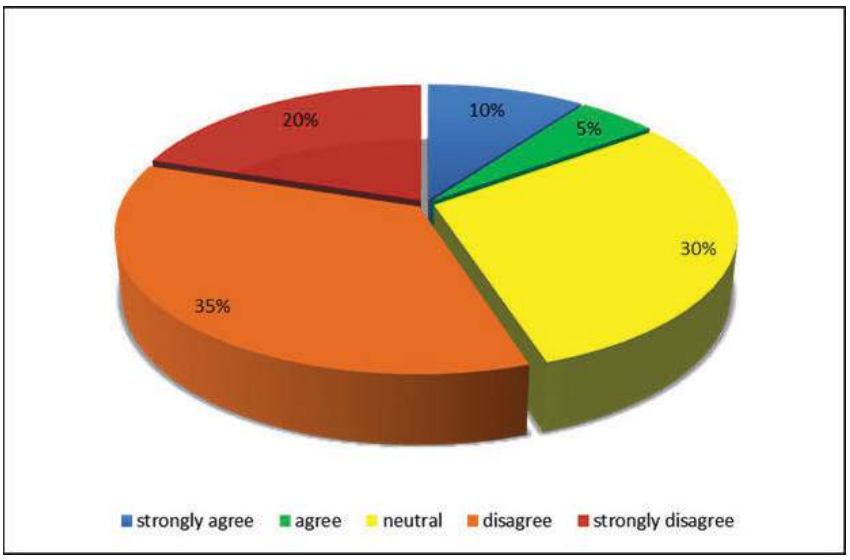

Figure 7: (Participants' Responses to the Seventh Questionnaire Item).

The pie chart in Figure 6 above shows that less than one quarter of participants (10% strongly agreed in blue and 5% agreed in green) believe that AI could cause boredom and reduce motivation to learn and teach. This view may stem from the idea that the lack of emotional connection and real human feedback in AI tools makes learning less personal, which can lower students' motivation and engagement. It might also be related to the fact that AI provides instant answers, which could make teachers and learners less active in thinking critically. Thirty percent of participants were neutral.

However, more than half of participants (35% disagreed in orange and 20% strongly disagreed in red) rejected the idea that AI causes boredom or frustration. These participants likely believe that AI can offer learning materials that fit individual learning styles, making learning more enjoyable and engaging instead of boring.

4.CONCLUSION

The study concluded that the majority of Libyan EFL instructors in the Department of Applied Linguistics at the Faculty of Languages in Benghazi during the 2024/2025 academic year had a positive attitude toward using artificial intelligence (AI) in their teaching. Instructors viewed AI as important for helping students enhance their language skills.

They believed AI encourages active participation and reduces the fear of making mistakes. Most instructors did not think AI causes boredom or lowers motivation; rather, they saw it as a tool that provides personalized learning materials to meet individual needs and boost engagement. However, many teachers reported facing challenges when using AI and primarily learned to use these tools through self-study.

Findings of this study were in consistence with Abolkasim and Hasan [23], whose study showed a strong interest in using AI tools in Libya's education system. However, some worries were raised about students becoming too dependent on AI tools, which might cause laziness and affect their honesty and creativity [23]. The results of this research also aligned with Hmouma [24], who found that EFL students support using technology to improve their English skills, and valued the quick feedback that AI offers. Despite this, several concerns were still expressed [24]. Finally, findings of this re-

search are somewhat similar to those of Alshumaimeri and Alshememry [22] who conducted a systematic examination for 80 papers from IEEE, Scopus, and Web of Science databases and found that AI tools were the most preferred applications among Liban EFL participants.

Findings of this study provide significant feedback to the head dean of the Faculty of Languages that it is crucial that AI tools be formally integrated in EFL classrooms. The study contributes to existing literature by examining teachers' perceptions of AI in an area not previously explored. It found that EFL Libyan teachers in the Department of Applied Linguistics at the Faculty of Languages have a positive attitude toward using AI in teaching. Moreover, these findings can guide future improvement initiatives in other similar Libyan EFL contexts. The researcher recommends that future research aim to find solutions to the identified AI challenges in this study. Additionally, educational procedures for effective integration of AI into classrooms provided in formal institutional programs are urgent to develop clear guidelines and ethical frameworks for AI use classrooms. Finally, this research is limited to teachers of Applied Linguistics at the Faculty of Languages in Benghazi, future research should be conducted in other Libyan EFL settings and focus on how AI can support the development of specific language skills, such as reading, writing, listening, and speaking.

5.ACKNOWLEDGMENT

I would like to sincerely thank my colleagues in the Department of Applied Linguistics at the Faculty of Languages, Benghazi University, as well as the administration, for their support and for granting me the opportunity to carry out this research.

REFERENCES

1. Lee D, Kim H, Sung SH. Development research on an AI English learning support system to facilitate learner-generated-context-based learning. Educ Technol Res Dev. 2023;71(2):629-66. https://doi:10.1007/s11423-022-10172-2

2. Jiang R. How does artificial intelligence empower EFL teaching and learning nowadays? A review on artificial intelligence in the EFL context. Front Psychol. 2022;13:1049401. https://doi:10.3389/fpsyg.2022.1049401

3. Criollo S, Guerrero-Arias A, Jaramillo-Alcázar Á, Luján-Mora S. Mobile learning technologies for education: benefits and pending issues. Appl Sci. 2021 May 6;11(9):4111. https://doi:10.3390/app11094111

4. Şad SN, Özer N, Yakar Ü, Öztürk F. Mobile or hostile? Using smartphones in learning English as a foreign language. Comput Assist Lang Learn. 2022;35(5-6):1031-57. https://doi:10.1080/09588221.2020.1770292

5. Zain DSM, Bowles FA. Mobile-assisted language learning (MALL) for higher education instructional practices in EFL/ESL contexts: a recent review of literature. Computer Assist Lang Learn Electron J. 2021;22(1):282-307. Available form: https://www.researchgate.net/publication

6. Christopher M. Artificial intelligence definitions. Stanford University Human Centered Artificial Intelligence [Internet]. 2020 [cited 2025 Jul 15]. Available from: https://hai.stanford.edu/sites/default/files/2020-09/AI-Definitions-HAI.pdf

7. Ejaz U, Godwin O. Ethical considerations in the deployment and regulation of artificial intelligence [Internet]. 2024 [cited 2025 Jul 15]. Available from: https://www.researchgate.net/publication/378070372

8. Chen X, Xie H, Zou D, Hwang GJ. Application and theory gaps during the rise of Artificial Intelligence in Education. Comput Educ Artif Intell [Internet]. 2020 [cited 2025 Jul 15];1:100002. Available from: https://doi.org/10.1016/j.caeai.2020.100002

9. Tang KY, Chang CY, Hwang GJ. Trends in artificial intelligence-supported e-learning: a systematic review and co-citation network analysis (1998–2019). Interact Learn Environments. 2023;31(4):2134-52. DOI:10.1080/10494820.2021.1875001

10. Zhai X, Chu X, Chai CS, Jong MSY, Istenic A, Spector M, et al. A review of artificial intelligence (AI) in education from 2010 to 2020. Complexity. 2021;2021(1):e8812542. https://doi:10.1155/2021/8812542

11. Schmidt T, Strassner T. Artificial intelligence in foreign language learning and teaching. Anglistik. 2022;33(1):165-84. https://doi:10.33675/angl/2022/1/14

12. Jeon G. Artificial intelligence approaches for energies. Energies. 2022;15(18):6651. https://doi:10.3390/en15186651

13. Kuning DS. Technology in teaching speaking skill. J Engl Educ Lit Linguist. 2019;2(1):50-9. https://doi:10.31540/jeell.v2i1.243

14. Akyuz Y. Effects of intelligent tutoring systems (ITS) on personalized learning (PL). Creative Education [Internet]. 2020 Jun 11 [cited 2025 Jul 15];11(6):953-78. Available from: https://doi.org/10.4236/ce.2020.116069

15. Korn J, Kelly S. New York City public schools ban access to AI tool that could help students cheat. CNN [Internet]. 2023 Jan 6 [cited 2025 Jul 15]. Available from: https://edition.cnn.com

16. Alharbi M. The role of artificial intelligence in advancing English as a foreign language teaching at Saudi universities. World J Educ Technol Curr Issues [Internet]. 2024 [cited 2025 Jul 15];16(3):181-200. Available from: https://doi.org/10.18844/wjet.v16i3.9311

17. Farahat A. Elements of academic integrity in a cross-cultural Middle Eastern educational system: Saudi Arabia, Egypt, and Jordan case study. Int J Educ Integrity [Internet]. 2022 [cited 2025 Jul 15];18:1-18. Available from: https://www.researchgate.net/deref/https

18. Civil B. ChatGPT can hinder students' critical thinking skills: Artificial intelligence is changing how students learn to write. The Queen's Journal [Internet]. 2023 [cited 2025 Jul 15]. Available from: https://www.queensjournal

19. Alhalangy I, AbdAlgane M. Exploring the impact of AI on the EFL context: a case study of Saudi universities. J Intercult Commun [Internet]. 2023 [cited 2025 Jul 15];23(2):41-9. Available from: https://doi.org/10.36923/jicc.v23i2.125

20. AbdAlgane M, Jabir Othman KA. Utilizing artificial intelligence technologies in Saudi EFL tertiary level classrooms. J Intercult Commun [Internet]. 2023 [cited 2025 Jul 12];23(1). Available from: https://papers.ssrn.com/sol3/papers.cfm?abstract_id=4565768

21. Holstein K, McLaren BM, Aleven V. Spacle: Investigating learning across virtual and physical spaces using spatial replays. ACM Int Conf Proceeding Ser. 2017:358-67. https://doi:10.1145/3027385.3027450

22. Alshumaimeri Y, Alshememry A. The extent of AI applications in EFL learning and teaching. IEEE Trans Learn Technol [Internet]. 2024 [cited 2025 Jul 15];17:653-63. Available from: https://doi.org/10.1109/TLT.2023.3322128

23. Abolkasim E, Hasan M. Integrating ChatGPT in education and learning: A case study on Libyan universities. Sebha Univ J Pure Appl Sci [Internet]. 2024 [cited 2025 Jul 15];23(2). Available from: https://doi.org/10.51984/JOPAS.V23I2.3082

24. Hmouma M. Exploring Libyan EFL undergraduates' attitudes towards AI-driven English learning applications. J Alzawia Univ Fac Educ [Internet]. 2024 [cited 2025 Jul 15];26:1-13. Available from: https://www.scribd.com/document/

25. Law L. Application of generative artificial intelligence (GenAI) in language teaching and learning: A scoping literature review. Comput Educ Open. 2024;6:100174. https://doi:10.1016/j.caeo.2024.100174

26. Ng DTK, Leung JKL, Chu SKW, Qiao MS. Conceptualizing AI literacy: An exploratory review. Comput Educ Artif Intell. 2021;2:100041. https://doi:10.1016/j.caeai.2021.100041

27. Kumar R. Research methodology: a step-by-step

guide for beginners. 4th ed. London: SAGE Publication Ltd; 2014.

28. Zamri NA, Purwati AS, Sudjono. The effect of profitability and leverage ratios on earnings per share (EPS): An empirical study on manufacturing companies listed on the Indonesia Stock Exchange in the year 2012-2015. Al-Tijary J Islam Econ Bus. 2016;1(2):151-66. https://doi:10.21093/at.v1i2.532

Applied Science

Scientific Journal of University of Benghazi

SJUOB (2025) 38 (2) Applied Sciences: Atawiry & kadi, 24 – 31
www.sjuob.uob.edu.ly

Structure of the even-even (220-230) Th isotopes within the Framework IBM-2

Mariam I.Atawiry [1]*, Sadiq M .El-kadi *(professor emaritus)* [2]

1.2. Physics Department,Faculty of Science,Tripoli University,Tripoli,Libya.

DOI: 10.37376/sjuob.v38i2 | Received:19/08/2025 | Accepted:31/11/2025 | Publishing: 23/12/2025

ABSTRACT

The specific In this study, some of the nuclear properties of the even-even thorium isotopes in the mass range A=(220–230) were studied within the interacting boson model (IBM-2) framework. The parameters in the Hamiltonian of the IBM-2 model were used to determine which one best fits the experimental spectrum. The NPBOS code was used to diagonalize this Hamiltonian, and the energy level was obtained. Our theoretical calculations and the latest experimental data showed a reasonable degree of agreement. From these calculations, it was possible to determine the dynamic symmetries of these isotopes based on several tests that rely in their calculations on energy levels. Based on the results of the tests used, The isotopes $^{(226-230)}_{90}Th$ were classified as having rotational symmetry SU(3), $^{224}_{90}Th$ had X(5) symmetry while the isotope $^{220}_{90}Th$ had vibrational symmetry U(5), and the isotope $^{222}_{90}Th$ had unstable gamma symmetry O(6). The phenomenon of backbending of these isotopes was studied, which only appeared in the isotope $^{220}_{90}Th$.

KEYWORDS: dynamic symmetries IBM-2 model, $^{(226-230)}_{90}Th$ isotopes.

Corresponding Author: Mariam I.Atawiry, mariamaltwairi51@gmail.com.

 ISSN: Online 2790-1637, Print 2790-1629
National Library of Libya, Legal number: 154/2018

1.INTRODUCTION

The study of nuclear collective motion through the spectroscopy of medium-mass and heavy even-even nuclei is one of the most fascinating areas of nuclear physics [1]. The atomic nuclei within the actinide region, particularly thorium isotopes in the mass range A=220–230, provide an excellent testing ground for investigating structural evolution in nuclear architecture. These isotopes reside in a transitional region between well-established nuclear collective spectra.

Many models were developed to study various nuclei because there was no standard theory that could be applied to all of them [2]. One of the main phenomenological approaches used within these models is the IBM-2 model, which effectively describes nuclear collectivity and collective motion in terms of bosons. Arima and Iachello [3] introduced the interacting boson model (IBM-2), one of the algebraic models for studying nuclear structure. Based on group theory, this model characterizes different kinds of nuclear collective states in even-even nuclei.

The bosons, which are pairs of identical valence nucleons with angular momenta of (J=0) for the s state or (J=2) for the d state, are treated as separate constituents, while the nucleus is regarded as an inner core. This model, which is based on algebraic Hamiltonians and is ideal for studying phase transitions, has been widely used to study nuclei from various mass regions. The nuclear shapes in this model that undergo the transition are linked to dynamic symmetries, which allow for the analytic solution of the pertinent observables [4].

The IBM-2 model allows for the replication of three distinct classes of nuclei that, according to standard nomenclature, correspond to axially symmetric deformed rotors, vibrational rotors, and γ-unstable rotor nuclei connected with subgroups in the group reduction process, which begins with the top group U(6) and are designated as SU(3), U(5) and O(6), respectively [5]. Since most collectively structured nuclei have mixed properties rather than just one symmetry, a new class of symmetries that apply to systems localized at critical points was proposed. A recent proposal describes nuclei at the points of phase transitions between various dynamical symmetries using the critical point symmetries E(5) and X(5). The phase transition from U(5) to O(6) is represented by the E(5) critical point symmetry, whereas the transition from U(5) to SU(3) is described by the X(5) critical point symmetry [6].

In the present study, we employed the IBM-2 model to calculate the low-lying energy levels of thorium isotopes in the mass range A = 220–230. The calculated results are compared with available experimental data. Many methods, such as the E-GOS curves, the back-bending, the ratio r(I+2/I) and ratio R(4/2) were used to identify and verify the general characteristics of these isotopes.

The Hamiltonian of the Proton-Neutron Interacting Boson Model (IBM-2)

In the IBM-2 model, the degrees of freedom of protons and neutrons are explicitly considered; therefore, the Hamiltonian can be expressed as [1,3,7]

$$\hat{H} = \varepsilon(\hat{n}_{d\pi} + \hat{n}_{dv}) + \kappa_{\pi v}\hat{Q}_{\pi}^{(2)}.\hat{Q}_{v}^{(2)} + \hat{V}_{\pi\pi} + \hat{V}_{vv} + \hat{M}_{\pi v} \quad (1)$$

Where ε is the d-boson energy, for proton $\varepsilon_{d\pi}$ and neutron ε_{dv} ,are assumed to be equal $(\varepsilon_{\pi} = \varepsilon_{v} = \varepsilon)$, $\hat{n}_{d\rho}$ $(\rho = \pi, \nu)$ is number operator of the d-bosons

$\kappa_{\pi v}$, is the strength of the quadrupole interaction between neutron and proton bosons, $\hat{Q}_{\rho}^{(2)}$ the quadrupole moment operator is given by:

$$\hat{Q}_{\rho}^{(2)} = (s_{\rho}^{\dagger}\tilde{d}_{\rho} + d_{\rho}^{\dagger}s_{\rho})^{(2)} + \chi_{\rho}(d_{\rho}^{\dagger}\tilde{d}_{\rho})^{(2)} \ldots\ldots (2)$$

χ_{ρ} is the quadrupole deformation parameter for neutrons $(\rho = \nu)$ and protons $(\rho = \pi)$, the term $\hat{V}_{\pi\pi}$ and $\hat{V}_{\nu\nu}$ represent the interaction between like-bosons, and they are written as:

$$\hat{V}_{\rho\rho} = \sum_{L=0,2,4} \frac{1}{2}\sqrt{2L+1}\, C_{L}^{\rho}\left[(d_{\rho}^{\dagger}d_{\rho}^{\dagger})^{(L)}(\tilde{d}_{\rho}\tilde{d}_{\rho})^{(L)}\right]^{(0)} + \kappa_{\rho\rho}\hat{Q}_{\rho}^{(2)}.\hat{Q}_{\rho}^{(2)} \ldots (3)$$

The last term in equation (3) is quadrupole interaction among similar bosons.

The Majorana operator is contained in the final term of equation (1) and is typically added to eliminate states of mixed proton- neutron symmetry. It is possible to write this term as[8][9]:

 ISSN: Online 2790-1637, Print 2790-1629
National Library of Libya, Legal number: 154/2018

$$\hat{M}_{\pi\nu} = \frac{1}{2}\xi_2\left(d_\nu^\dagger s_\pi^\dagger - s_\nu^\dagger d_\pi^\dagger\right)^{(2)}.\left(\tilde{d}_\nu s_\pi - s_\nu \tilde{d}_\pi\right)^{(2)} - \sum_{k=1,3} 2\xi_k\left(d_\nu^\dagger d_\pi^\dagger\right)^{(k)}.\left(\tilde{d}_\nu \tilde{d}_\pi\right)^{(k)} \quad \ldots\ldots\ldots\ldots\ldots\ldots(4)$$

Energy Ratios and Nuclear Shape Transition

Nuclear shape phases are manifestations of the collective motion modes in nuclei. Consequently, numerous methods have been developed to study and identify these symmetries [6].

Energy Ratio R (4/2)

The energy ratio R (4/2) between the first 2_1^+ and excited states serve as a key indicator of nuclear shape transitions along isotopic chains. It ranges from R (4/2) = 2 for vibrational nuclei near spherical shapes, to R (4/2) = 3.33 for deformed rotor, and R (4/2) = 2.5 for γ-soft nuclei [10].

E-GOS Curves

The relation R=Eγ (I→I−2)/I, known as the E-GOS (Energy Gamma Over Spin) curve, was introduced by Regan et al. [10]. It effectively highlights vibrational and rotational behaviors, as well as transitions between them, without requiring prior structural assumptions.

The information provided by this relation is valuable for understanding structural evolution along the yrast line in even-even nuclei. For the three limiting cases, the E-GOS relations are given by [11]:

$$(\text{Vibrational})\ \ R(I) = \frac{\hbar\omega}{I} \xrightarrow{I\to\infty} 0 \quad \ldots\ldots,(5)$$

$$(\text{Rotational})\ R(I) = \frac{\hbar^2}{2J}\left(4 - \frac{2}{I}\right) \xrightarrow{I\to\infty} 4\left(\frac{\hbar^2}{2J}\right) \ldots\ldots(6)$$

$$(\gamma - \text{soft})\ \ R(I) = \frac{E_{2_1^+}}{4}\left(1 + \frac{2}{I}\right) \xrightarrow{I\to\infty} \frac{E_{2_1^+}}{4} \ldots\ldots(7)$$

The Ratio $\mathbf{r\left(\frac{I+2}{I}\right)}$.

The symmetry for the excited band of even-even nuclei was defined by constructing the following ratios for a given for each spin.

$$r\left(\frac{I+2}{I}\right) = \left[R\left(\frac{I+2}{I}\right)_{exp} - \frac{I+2}{I}\right] \times \frac{I(I+1)}{I(I+2)} \ldots\ldots(8)$$

The properties of each nucleus were ascertained by applying this relationship to a collection of distinct nuclei, where $R\left(\frac{I+2}{I}\right)_{exp}$ is the experimental value of the ratio in equation (8) [11]. by the limits $0.1 \le r \le 0.35$ for the vibrational nuclei, $0.4 \le r \le 0.6$ for the γ-unstable nuclei, and $0.6 \le r \le 1$ for the rotational nuclei.

The Back-bending Phenomena.

This phenomenon was discovered by Johnson et al. [12]. They observed that a significant increase in the moment of inertia at a specific angular momentum was accompanied by a decrease in the energy of the Gamma-transition connecting states with spin I and I-2 in certain nuclei [13]. This effect causes the value of $\hbar\omega$ to backbend, as quantified in reference [2].

$$\hbar\omega = \frac{\Delta E}{\sqrt{I(I+1)} - \sqrt{(I-2)(I-1)}} \ldots\ldots,(9)$$

And the immediately of inertia is given by:

$$\frac{2\vartheta}{\hbar^2} = \frac{4I-2}{\Delta E} \quad \ldots\ldots,(10)$$

Where $\Delta E = E(I) - E(I-2)$

2.RESULTS AND DISCUSSION

Energy Levels

The isotopes $^{(220-230)}_{90}Th$ have $N_\pi = 4$ and N_ν varies from 2 to 7. Tables 1 and 2 list the Hamiltonian parameters best fit values. Theoretically, one nucleus energy spectrum can be fitted by varying each parameter separately. The values of the parameters were chosen, and one parameter was then allowed to change while the others remained constant until the best fit was achieved. Iteratively, this process was continued until a general fit was obtained. After choosing the proper parameters for each isotope, we applied the Hamiltonian of IBM-2 to our study in order to calculate the theoretical values of energy levels. For numerical calculation, the computer program NPBOS is used to diagonalize the IBM-2 Hamiltonian and generate energy space[14].

Table 1. the best fit values of the Hamiltonian parameters for .

$^{A}_{Z}X_{N}$	$^{220}_{90}Th_{130}$	$^{222}_{90}Th_{132}$	$^{224}_{90}Th_{134}$
ε	1.091		
κ	-0.089	0.940	1.096
χ_π	3.460	-0.089	-0.093
χ_ν	2.232	2.924	1.804
$CL_\nu(L=0)$	-0.278	2.350	2.100
$CL_\nu(L=2)$	-0.189	-0.297	-0.353
$CL_\nu(L=4)$	-0.362	-0.091	-0.151
$CL_\pi(L=0)$	1.655	-0.295	-0.267
$CL_\pi(L=2)$	-0.041	0.899	-0.255
$CL_\pi(L=4)$	-0.161	-0.189	-0.173
ξ_1	2.200	0.010	-0.110
ξ_2	-0.089	0.250	0.250
ξ_3	2.209	-0.165	-0.145

Table 2. the best fit values of the Hamiltonian parameters for.

$^{A}_{Z}X_{N}$	$^{226}_{90}Th_{136}$	$^{228}_{90}Th_{138}$	$^{230}_{90}Th_{140}$
ε	0.940	0.977	0.977
κ	-0.089	-0.089	-0.089
χ_π	5.741	5.335	5.341
χ_ν	2.459	2.530	2.450
$CL_\pi(L=0)$	0.819	0.940	0.930
$CL_\pi(L=2)$	0.469	0.372	0.311
$CL_\pi(L=4)$	-0.112	-0.152	-0.147
$CL_\nu(L=0)$	0.420	0.690	0.690
$CL_\nu(L=2)$	0.420	0.130	-0.001
$CL_\nu(L=4)$	-0.390	-0.310	-0.295
ξ_1	1.790	0.970	0.950
ξ_2	-0.164	-0.130	-0.131
ξ_3	1.509	1.090	1.090

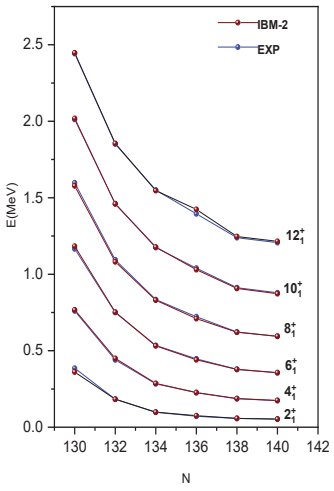

Figure 1: Comparison the experimental and IBM-2 calculated energy levels of ground state band for $^{(220-230)}Th$ isotopes $[15-20]$.

The Figure. 1 displays both the experimental energy and the estimated energy levels in the ground states band for $^{(220-230)}Th$ isotopes using the parameters in the Table 1As demonstrated, there have a good degree of agreement between experimental and theoretical values of the energy levels.

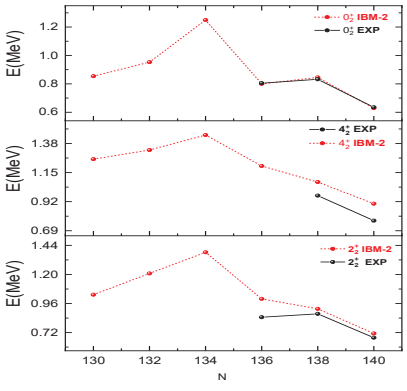

Figure 2: Comparison the experimental and IBM-2 cal-

culated energy levels of $\gamma-$band , and beta band for 2_2^+ , 4_2^+ states and 0_2^+ state respectively. for $^{(220-230)}$Th isotopes $[15-20]$.

The Figure 2: shows the available experimental and calculated energy levels in the beta band for 0_2^+ state and the $\gamma-$band for 2_2^+ , 4_2^+ states for the $^{(220-230)}$Th isotopes , results were obtained that were in reasonable agreement with experimental calculations.

Dynamical Symmetry of Thorium Isotopes $^{(220-230)}_{90}$Th. .

1. Energy Ratios R (4/2).

To characterize the evolution of collectivity in the thorium isotopic chain, we examined the energy ratio R(4/2). The thorium isotopes change from a vibrational structure to a rotational one as the number of neutrons increases, as seen in Figure 3.

The findings showed that isotopes $^{(226-230)}$Th had properties of SU(3) symmetry, whereas ^{222}Th and ^{220}Th follow the O(6) and U(5) limits, respectively. The isotope ^{224}Th lied at the critical point defined by the X(5) symmetry.

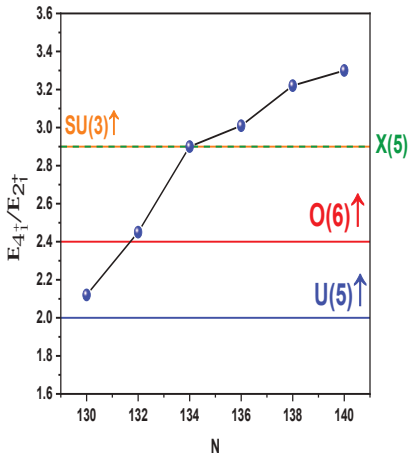

Figure 3: The ratio $\frac{E_{4_1^+}}{E_{2_1^+}}$, $^{(220-230)}$Th of isotopes.

2.E-GOS Curves.

In this study, we plotted $E-GOS$ curves using data for the ground states band of the even-even nuclei extending from $^{220}_{90}$Th to $^{230}_{90}$Th .We compared the $E-GOS$ curves with the ideal limits for a harmonic oscillator, where the first excited state is located at an energy of $E_{2_1^+}$ = 500 Kev , an axisymmetric rotor is located at an energy of $E_{2_1^+}$ = 100 Kev, and the γ-soft at energy $E_{2_1^+}$ =300 Kev .

As shown in Figure 4, the comparison with these ideal symmetry limits reveals a clear pattern. The E-GOS curves for isotopes $^{(224-230)}$Th consistently align with the SU(3) symmetry across all spin (I) values. Furthermore, the curve for ^{222}Th matches the O(6) symmetry, while that of ^{220}Th Th corresponds to the U(5) limit.

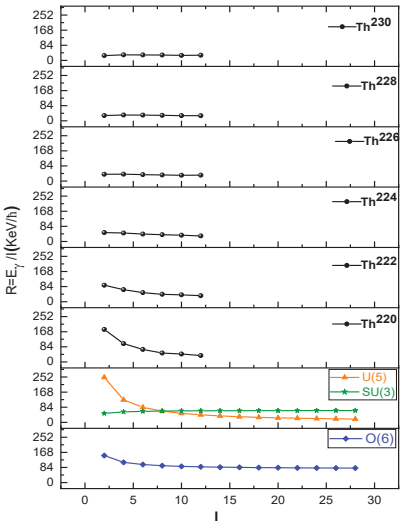

Figure 4: Comparison of the $E-GOS$ curves for the ground states band of $^{(220-230)}_{90}$Th isotopes calculated with the $E-GOS$ curves for the three standard states $U(5), O(6),$ and $SU(3)$.

3. The Ratio $r(\frac{I+2}{I})$.

Figure 5 presents the calculated ground-state band for the thorium isotopes $^{(220-230)}$Th . The behavior of

the ratio r as a function of spin *I* for each isotope can be observed and interpreted.

For the vibrational-like nuclei ^{220}Th and ^{222}Th, the r ratios begin at a low value and increase with spin *I*. In, ^{220}Th some negative r values are observed. This can be attributed to the isotope's near-spherical magic properties, as its neutron number *N*=130 is close to the magic number *N*=126.

According to our analysis, ^{224}Th is interpreted as a critical-point nucleus. Consequently, its properties are consistent with the X(5) dynamical symmetry, which describes nuclei at the transition between spherical and deformed shapes.

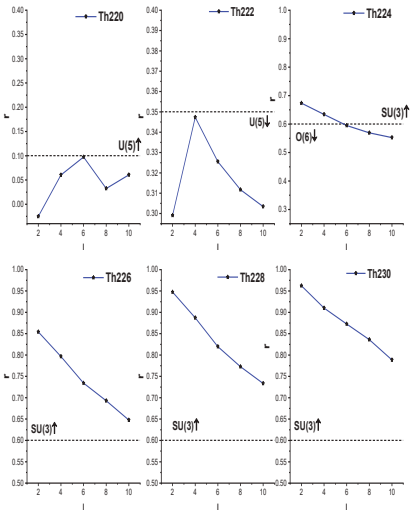

Figure 5: The ratio r((I+2)/I) as a function of I for the even-even isotopes of thorium $^{(220-230)}_{90}\mathrm{Th}$.

For the heavier isotopes $^{(226-230)}\mathrm{Th}$, the r values align with the characteristic pattern for a rotational nucleus. They start with a value close to unity and exhibit a steady decrease with increasing spin *I*.

4. The Back-bending Phenomena

To investigate the phenomenon of back-bending, we plotted the moment of inertia, $\frac{2\vartheta}{\hbar^2}$ as a function of the square of the photon energy $(\hbar\omega)^2$ emitted when the nucleus transitions from state I to state I-2, for the thorium isotopes $^{(220-230)}\mathrm{Th}$. This relationship, shown in Figure. 6, reveals that backbending occurs only in $^{220}\mathrm{Th}$. For this isotope, the backbending phenomenon is observed at spins I = 8 and I = 12.

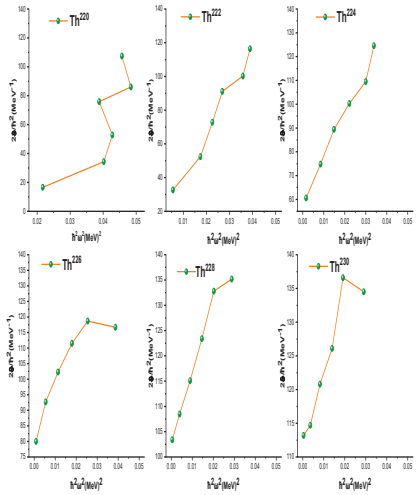

Figure 6: Moment of inertia as a function of the square of the rotational energy for the isotopes $^{(220-230)}_{90}\mathrm{Th}$.

3.CONCLUSION

In this study, we employed the Interacting Boson Model (IBM-2) to systematically investigate the structural properties of thorium isotopes across the mass range (A=220-230). Our analysis revealed that the IBM-2 framework successfully described the nuclear structure evolution throughout this isotopic chain.

The calculations were performed using a neutron-proton boson code (NPBOS). The computed excitation energies showed good agreement with experimental data for members of the ground-state band, the γ-band, and the β-band.

To determine the dynamic symmetries of each isotope, we analyzed the E-GOS curves, the R(4/2) ratio, and the r(I+2/I) ratio. Our analysis indicated that $^{220}_{90}\mathrm{Th}$ exhibits characteristics of the U(5) dynamical symmetry. The $^{222}_{90}Th$ showed O(6) symmetry, $^{224}_{90}Th$ had X(5) symmetry, while the heavier isotopes $^{(226-230)}Th$

 ISSN: Online 2790-1637, Print 2790-1629
National Library of Libya, Legal number: 154/2018

rotational symmetry SU(3).

Furthermore, the back-bending phenomenon was observed only in the $^{220}_{90}Th$ isotope, occurring at spin values of I=8 and I=12.

4.ACKNOWLEDGEMENT

We would like to thank Dr. Taher Al-Sharif and Dr. Mohamed Abdel Aziz for contributing to the analysis of some equations related to the dynamic symmetries of the IBM-2 model.

REFERENCES

1.Scholten,O .The interacting boson Approximation Model and Applications,Netherlands:Rijksuniversiteit Groningen.1980.

2.Imad A. Abed Al-Jubbori M . Kassim H . Hewa Y. Sharrad F .(2018) 'Investigation of even - even isotopes within the IBM , IVBM and BM. Nucl .phys. A . 2018. Vol.977. p.34-48 .Available from: doi: 10.1016/j.nuclphysa.2018.05.010;

3. Arima A.Iachello F.the Interacting boson model'. united kingdom: Cambridge university .1987.

4.Giannatiempo A . Heavy neodymium isotopes in the interacting boson (IBM-2) model.Phys. Rev.C..2011.84,024308. Available from:DOI: https://doi.org/10.1103/PhysRevC.84.024308

5. Youn S. Young J and Lee J.the study of structure in 224-234 thorium nuclei with the framework IBM. EPJ Web of Conferences. .2017. 146, 10016. Available from:doi:https://doi.org/10.1051/epjconf/201714610016

6. Khalaf A.Ismail A. structure shape evolution in lanthanide and actinide nuclei.progress in physics .2013 April. ISSN 1555-5615 . Available from: chrome-extension://efaidnbmnnnibpcajpcglclefindmkaj/https://progress-in-physics.com/2013/PP-33-15.PDF

7.Sarangi S and Parikh J. Dynamic microscopic basis for IBM-2 : a new approach. Pramana . .1993 January .40(1). p. 43–57. Available from: https://link.springer.com/article/10.1007/BF02898041

8. Igal T. Simple Of Complex Nuclei : The Shell Model and Interacting Boson Model . In : Herman Feshbach, editors .Contemporary Concepts in Physics.,harwood academic publishers : Switzerland. 1993. p.867-895.

9. Casten R.Lipas P. warner D . Otsuka T . Heyde K .Darayer J. Algebraic Approaches to Nuclear Structure .In: Herman Feshbach,editors Contemporary concepts in physics . harwood academic Publishers : Switzerland. 1993. p.4-245.

10. Regan P.Beausang C.Zamfir N.Casten R.Jing-ye-zhang.Yamamoto A.Caprio M.G G.Hech A.Signature for vibrational to rotationalevolution along the yrast line. Phys. Rev. Lett . 2003. 90, 152502 Available from: doi: https://doi.org/10.1103/PhysRevLett.90.152502.

11. Abed al- jubbori M. investigation of energy levels and electromagnetic transitions for Yb – Pt nuclei with N=108 using IBM ,IVBM ,and BMM .Ukrainian journal of physcs . 2017. 62 .11, 936. Available from:doi: 10.15407/ujpe62.11.936

12. Johnson A. Ryde H. and Sztarkier J. Evidence for a "singularity" in the nuclear rotational band structure ,phys. Let. B. .1971. Volume 34, Issue 7, p.605-608. Available from: https://doi.org/10.1016/0370-2693(71)90150-X

13. Al-alawy I.Salman K.Aobaid A. Back bending phenomena evaluation and energy band crossing of some deformed nuclei, researchgate .2016 January. Available from: https://www.researchgate.net/publication/332571166_Back_bending_phenomena_evaluation_and_energy_band_crossing_of_some_deformed_nuclei#fullTextFileContent

14. Otsuka T. Yoshida N . user's manual of the program NPBOS , Japan atomic energy research institute..1985 July.Available from: https://inis.iaea.org/records/zafwd-kk464

15.Singh B. Sing S.Nuclear Data Sheets For . Upton. New York:Brookhaven National Laboratory.2022. Available from: https://www.nndc.bnl.gov/ensdf/EnsdfDispatcherServlet

16. Browne B.Tuli J.Nuclear Data Sheets For . Upton. New York:Brookhaven National Laboratory . 2012. Available from: https://www.nndc.bnl.gov/ensdf/EnsdfDispatcherServlet

17. Browne E. Tuli J.(2014) Nuclear Data Sheets For ,Upton,New York:Brookhaven National Laboratory . . 2014. Available from: https://www.nndc.bnl.gov/ensdf/EnsdfDispatcherServlet

18. Abusaleem K.(2014) Nuclear Data Sheets For . Upton.New York :Brookhaven National Laboratory.2014. Available from: https://www.nndc.bnl.gov/ensdf/EnsdfDispatcherServlet

19. Singh S. Jain A. Jagdish K.Tuli K. Nuclear Data Sheets For , Upton,New York:Brookhaven National Laboratory . .2011. Available from: https://www.nndc.bnl.gov/ensdf/EnsdfDispatcherServlet

20. Akovali Y.(1996) Nuclear Data Sheets For . Upton .New York :Brookhaven National Laboratory. .1996. Available from: https://www.nndc.bnl.gov/ensdf/EnsdfDispatcherServlet

21. Yang J.Lei-Wang H . Chai Q. Lin M.Rongxu F. Evolution of Shape and Rotational Structure in neutron-deficient {118-128}Ba Nuclei. Progress of Theoretical and Experimental Physics . .June 2016, , Issue 6 .063D03. Available from: https://doi.org/10.1093/ptep/ptw074

Scientific Journal of University of Benghazi

SJUOB (2025) 38 (2) Applied Sciences: Bashic & Matter, 32 – 42
www.sjuob.uob.edu.ly

Isolation of Candida albicans and Evaluation of Plant Extracts for Antifungal Activity.

Aisha M. El-Bashic[1], Hamdy AB. Matter[2 3] *

1.Biology Department, Banghazi University, El-Wahat, Jalo, Libya.
2.Chemistry Department, Banghazi University, El-Wahat, Jalo, Libya.
3.High Institute of Engineering and Technology, El-Arish, Egypt.

DOI: 10.37376/sjuob.v38i2 | Received:23/08/2025 | Accepted:21/11/2025 | Publishing: 23/12/2025

ABSTRACT

Candida albicans (C. albicans) is a common opportunistic fungal pathogen trustworthy for a variety of infections, especially in immunocompromised individuals. The increasing resistance to antifungal agents necessitates the search for alternative treatment options. In this study, we isolated C. albicans from clinical and environmental samples and evaluated several plant extracts, such as Allium sativm, salvia rosmarinus, Mentha, which we believed possessed antifungal activity. These plant extracts were tested for their ability to inhibit C. albicans growth using standard laboratory assays. Various plant extracts, including Allium sativm, salvia rosmarinus, Mentha yielded very similar results in terms of fungal inhibition, with the exception of the disc impregnated with peppermint extract, where no area of inhibition was observed. Several extracts exemplified promising inhibitory effects on fungal growth, suggesting that compounds derived from Allium sativm, salvia rosmarinus, Mentha could offer useful possibility or complement to current antifungal treatments. These findings paved the way for growth of plant based therapies to conflict drug reluctant fungal infections. The extracts exhibited great antifungal effects, notice on their potential as natural curative agents. These findings would assist further research into plant compounds as other possibility or complements to traditional antifungal drugs.

KEYWORDS: Candida albicans, Antifungal resistance, Allium sativm, salvia rosmarinus, Mentha, Natural antifungal agents, and Fungal pathogens.

Corresponding Author: Hamdy AB. Matter, hamdy.matter@uob.edu.ly

 ISSN: Online 2790-1637, Print 2790-1629
National Library of Libya, Legal number: 154/2018

1.INTRODUCTION

Candida albicans(C. Albicans) is the most common causative agent of candidiasis, a fungal disease in humans. It is found as a commensal organism in the microbiome of mammals and can cause superficial infections in healthy individuals and severe disease in immunocompromised patients. C. albicans infections are associated with high morbidity and mortality, particularly among chronically ill and critically ill patients. The pathogen undergoes a morphological transformation from yeast to filamentous forms, leading to infection. The path to treatment remains long due to the increasing drug resistance of fungi, their small numbers, and their limited efficacy. Most antifungal treatments target azoles and ergosterol, a major amphiphilic lipid and a fundamental component of the fungal plasma membrane. However, resistance and tolerance to azole are becoming an increasing problem. In C. albicans, ergosterol-rich membrane domains are thought to interact with sphingolipids and membrane proteins, including multidrug transporters, further complicating treatment strategies.

The interaction between Candida albicans (C. albicans) and host cells is mediated by a range of virulence factors, including adhesions and invasins, secretion of hydrolytic enzymes, morphological transformation from yeast to filamentous fungal hyphae, and the formation of a robust biofilm. These properties collectively smooth efficient adhesion, invasion, and damage to host tissues [1]. Three bioactive compounds isolated from bogostemon axillaris have indicate potent inhibitory activity against fluconazole resistant C. albicans (MIC = 4 µg/ml). The main compound, pachisamin M, disrupted ergosterol synthesis and exhibited strong antifungal activity both in vitro and in vivo, suggesting that pachisamin M may be a promising compound for overcoming antifungal resistance, particularly in C. albicans [2]. The tannin rich N-butanol fraction extracted from plant extracts also exhibits antifungal and anti-biofilm activity, effectively and efficiently preventing C. albicans infections. [3] Hexane (Hex) and dichloromethane (DCM) extracts from the roots of tridax pentachaeta also exemplify strong photosynthetic activity against C. albicans. [4] Bacterial perfringolicin serves as a direct indicator for monitoring the cellular effects of fluconazole, revealing that highly polarized ergosterol distribution is not prerequisite for budding or filamentous growth in C. albicans. [5] Genetic or pharmacological inhibition of the tyrosine phosphorylation moderate dual kinase (DYRK) Yak1 productively prevents C. albicans spore formation and biofilm formation. [6] Calcium-activated calcineurin^{+}-calmodulin phosphatase plays a pivotal role as an inhibitor of key stress response pathways in C. albicans, reducing fungal persistence and its ability to cause disease within the host [7]. Heat shock protein 90 (Hsp90) is a highly conserved molecular cofactor that regulates the folding, stability, and function of a wide range of client proteins, many of which are substantial for signal transduction and stress responses in C. albicans. The Ras1-cAMP-PKA and MAPK chains, which control splicing and stress adaptation, are important for the fungus. Hsp90 contributes to resistance to antifungal agents, such as calcineurin, enhancing the host's tolerance to drug-induced stress. Hsp90 dysfunction affects morphogenesis, biofilm formation, and virulence in vivo, making it an attractive target for antifungal drug. Inhibiting fungal Hsp90, particularly in integration with existing antifungal agents, offers significant potential for numerous drug efficacy and overcoming fungal drug resistance mechanisms without affecting the host Hsp90, given the structural differences between fungal and human forms [8]. Baicalin (BE) is a small-molecule antifungal compound make distinctive by broad-spectrum activity, synergistic interaction with fluconazole, and low toxicity. Recent findings indicate that BE has antifungal activity against C. albicans by disrupting glycolysis. More specifically, BE targets and inhibits enolase 1 (Eno1), a key enzyme in glycolysis [9]. High-intensity violet light was applied to specific yeast species, including C. albicans. Cell suspensions were exposed to narrowband violet light with a wavelength of 405 nm, generated by an LED array. All fungi were

 ISSN: Online 2790-1637, Print 2790-1629
National Library of Libya, Legal number: 154/2018

effectively and efficiently inactivated using light with a wavelength of 405 nm without the need for external photosensitizers [10].

Exposure to tunicamycin induces a specific chromosomal aberration, a chromosomal abnormality resulting from endoplasmic reticulum (ER) tension, leading to trisomy 2 (Chr2x3) in C. albicans. This confers cross-tolerance to caspofungin, an antifungal agent from the echinocandin family [11]. Phosphatidylserine phosphatases are key enzymes in lipid metabolism, catalyzing the conversion of phosphatidic acid to diacylglycerol. In C. albicans, phosphatidylserine phosphatase Pah1 plays a crucial role in fungal physiology [12]. Two aminotransferases have been identified in C. albicans, Aro8p and Aro9p, each with distinct catalytic properties that play an important role in inhibiting fungal growth [13]. bioactive compounds as gold nanoparticles (Ca_AuNPs) used by C. albicans exhibit anti-azole activity, including against fluconazole, itraconazole, and voriconazole, making them effective against multidrug-resistant C. albicans strains [14]. The alginate CD aptamer complex nanosensor shows pledge in clinical applications, offering a sensitive and environmentally friendly alternative to conventional methods for diagnosing C. albicans [15]. Tested antifungal proteins (AFPs) have demonstrated significant antifungal activity against cutaneous C. albicans infections [16]. Results have shown that the crude methanolic extract of turmeric exhibits antifungal activity against C. albicans [17]. A series of novel 5-phenylthiophene derivatives have been designed and synthesized to address the high incidence of drug-sensitive and drug-resistant fungal infections [18]. Ethyl acetate exhibited fungicidal activity against C. albicans at a concentration of 1.0 mg/ml [19]. The incorporation of a photofluorescent protein with random optical oscillation (SOFI) effectively inhibited background fluorescence. Histone acetyltransferase is essential for achieving full virulence, and Erg11, a target of azole antifungals, has been identified in C. albicans [20]. Poly ([2 - (methacryloyloxy) ethyl) trimethylammonium chloride cross-linked) (PMETAC) and bacterial cellulose nanoparticles (BNCs) were used to determine their antifungal activity against C. albicans polymorphotypes [21]. 2,4-Dietyr-butylphenol, an antibiotic, has shown efficacy and safety against C. albicans and other pathogenic fungi [22]. Necessary oils have been tested against C. albicans [23]. Proteins of aspergillus fumigatus and aspergillus albicans, which are expressed or activated during environmental changes and compression conditions, have been used to detect potential virulence factors [24]. A microfluidic chip has been designed and fabricated for the fast and perfect detection of aspergillus albicans in clinical samples, and its potential has been utilized for early and accurate diagnosis [25]. Using molecularly printed polymers (MIPs) enhanced with nickel, iron oxide ($NiFe_2O_4$) nanoparticles, a novel electrochemical biosensor has been fabricated for the fast and accurate detection of aspergillus albicans [26]. A CRISPR-based platform targeting the internal interleaving gene 2 (ITS_2) of aspergillus albicans has been developed. This method combines Cas12a DNase cleavage activity with recombinant polymerase (RPA) amplification for fast and accurate detection [27]. Berberine inhibits the expression of azole impedance genes in fungi, reduces cell adhesion, and damage biofilm formation. Gene transcription analysis suggests that interference with the iron gain pathway is a key mechanism underlying berberine's inhibition of drug resistant fungal strains [28]. When PG, CA, and CAR compounds were individually applied to C. albicans biofilms for 5 minutes, their viability decreased by less than 0.50 at both 5 °C and 22 °C [29]. The yeast form of C. albicans utilizes glycosaminoglycans (GAGs), particularly heparan sulfate, as receptors for adhesion to corneal epithelial cells [30].

2.METHODOLOGY

2.1. Isolation of *C. albicans*

2.1.1.Sample Collection:

Clinical or environmental samples suspected to contain C. albicans species were collected using sterile cotton swabs.

 ISSN: Online 2790-1637, Print 2790-1629
National Library of Libya, Legal number: 154/2018

2.1.2.Culturing:

Samples were inoculated on sabouraud dextrose agar (SDA) plates and incubated at 30 – 37°C for 24 – 48 hours.

2.2. Materials used:

Plastic Petri dishes (9 and 6 cm in diameter), isolation needle, forceps, pipettes, assorted cups, cotton, cellophane paper, punch, filter paper, sterile swabs, a culture medium consisting of sabouraud dextrose agar, lactophenol blue cotton stain, distilled water, Parafilm, microscope slides and coverslips, and ethyl alcohol.

2.3. Equipment used:

Autoclave, balance, cooler, incubator, water bath, isolation chamber, microscope, Bunsen burner, and heat sterilizer.

2.4. Plant material:

The following plants were dried: garlic, rosemary, and wild mint (Allium sativm, salvia rosmarinus and Mentha). They were purchased from a local farm in Ujla, Libya, and identified by a farmer and vendor based on their color and aroma.

2.5. Preparation of plant extracts:

2.5.1. Aqueous extracts (cold):

To prepare the aqueous extract, Allium sativm, salvia rosmarinus and Mentha from garlic, rosemary, and mint plants were dried, then chopped into small pieces and ground in a ball mill to a powder. The powder was divided into several 10-gram portions, placed in a sterile screw-cap bottle, and 100 ml of sterile deionized distilled water was added. The extract was left to infuse for 48 h at 4 °C before the mixture was centrifuged at 2000 r.p.m for 10 min. The supernatant was passed through a 0.45 mm diameter membrane sieve. The extract was stored in sterile screw-cap bottles in the refrigerator until needed. Aqueous extracts were prepared using sterile distilled water for each plant.

2.6. Preparation of the inoculum for testing:

The inoculum was prepared by suspending a few fungal colonies in test tubes containing 9 ml of sterile normal saline. The turbidity of the fungal suspensions was visually matched to the equivalent turbidity of a $BaCl_2$ standard, which has a similar appearance to broth culture.

2.7. Antifungal activity testing using the disc diffusion method:

The modified agar diffusion method was used to determine antimicrobial activity. Sabouraud dextrose agar was inoculated with a microbial cell suspension (200 µL in 20 mL of medium) and poured into sterile Petri dishes. Sterile 6 mm diameter filter paper discs were impregnated with 20 µL of each extract, prepared using the same solvent used to dissolve the plant extracts. The aqueous extract was then sterilized by pasteurization and membrane filtration and placed on the surface of the inoculated agar. The plates were incubated at 30–37 °C for 4 –7 days. At the end of the incubation period, antimicrobial activity was assessed by measuring the inhibition zones [31].

2.8. Sample Collection , Fungi used, C. albicans, Fungi isolated from vagina

Samples collected for several persons from Awjila AL-qrawi Hospital and Red Crescent Clinic Jalo in June, May, and April 2025year.

This is done by taking a sample of vaginal secretions or a thin layer of the crust covering the dermatitis by Fungi C. albicans.

2.9. Work methods:

Culture media used for the growth and isolation of C. albicans fungus sabourud dextros agar of the medium consists of agar 65 g, the medium powder is weighed using a sensitive balance (the quantity is usually recorded on the package) then 1000 ml of distilled water is added to the medium. The contents are mixed well and then placed in a water bath for a period (35- 40 min.) until the contents are well dissolved and become transparent. The mixture is then distributed into small 250 ml beakers to facilitate the process of pouring into dishes. These beakers are sterilized in an autoclave for 15-20 min., after which they are ready to be poured into Petri dishes.

Isolation of C. albicans fungus from some patients visiting the " Isolation of a fungus from some patients at-

 ISSN: Online 2790-1637, Print 2790-1629
National Library of Libya, Legal number: 154/2018

tending Awjila AL-qrawi Hospital and Red Crescent Clinic Jalu ". Samples were taken from patients who complained of infections in the vaginal area in general at different intervals, by taking a swab from the infected area and culturing it on special nutritional media represented by the sabouraud dextros agar medium, which is a special medium for the growth of C. albicans fungi.

It was then placed in an incubator at a temperature of 30-37 °C. The plates were monitored periodically for 4 -7 days to observe the growing colonies. The plates were then incubated. After this, the plates were ready for microscopic examination.

A small percentage of the fungus growth is taken with an isolation of fungal growths from the nutrient media using a sterile isolation needle. The fungal smear is placed on a glass slide with a drop of phenolic blue cotton stain and covered with a glass slide cover for microscopic examination. The sample is examined under different power of the light microscope (X 10 ،X 40, and X 100) The obtained characteristics, both macroscopic and microscopic, were compared with the previously identified isolate and the results were recorded.

2.10. Preparation of tablets saturated with extract:

5 mm diameter discs were made from sterilized filter paper, these discs were dipped in plant extracts according to the species for 5 min. After removing them, the discs were placed in Petri dishes containing growths of the fungus under study, 5 discs were distributed in each dish, so that each disc was at a distance from the fungal growth. The dishes were left at 30-37 °C and monitored periodically for 4 - 7 days, and the results were recorded .[32]

2.11. Minimum inhibitory concentration (MIC) and minimum bactericidal concentration (MBC):

Antifungal activity of Allium sativm, Salvia rosmarinus, and peppermint extracts on the growth and inhibition of C. albicans. For this experiment, we prepared 45 tablets of each Allium sativm, Salvia rosmarinus, and peppermint extract. Fifteen tablets were 100 % Allium sativm, 15 tablets were 100 % Salvia rosmarinus extract, and 15 tablets were 100 % peppermint extract. Five tablets were placed in each of three Petri dishes, each of which was left to contain a quantity of the extracts for 5 min. until saturated. Nine Petri dishes were prepared for testing, three for each extract. The dishes were inoculated with C. albicans at five locations on each dish. The discs were taken and distributed onto plates, each disc placed at a distance from the fungal isolate. The plates were incubated in an incubator at 30-37 °C. The plates were monitored after 4 -7 days in the incubator, and the results were recorded.

The MIC is defined as the lowest concentration of aqueous extracts capable of inhibiting fungal growth. Sabouraud dextrose broth was used to determine the MIC in the preparation of serial dilution test tubes. Serial dilutions of the two extract samples were performed in test tubes containing 2 ml of sabouraud dextrose broth medium to yield final concentrations of 2:2, 2:4, 4:6, and 6:8 mg/mL. 20 µl of the test organisms (108 CFU/ml) were distributed into the tubes. The negative control tube contained only 2 ml of the two extracts but did not contain any organisms. Positive control tubes contained only 2 ml of broth medium and each of the organisms, but neither extract was present. The tubes were incubated at 30 – 37 °C for 4 – 7 days. After incubation, the turbidity of each tube was visually checked. The clear test tube indicated the breakage point. From tubes showing no visible sign of growth / turbidity in the MIC determination, the test micro-organisms were inoculated onto sterile sabouraud dextrose agar plates using the stripe plate method. The plates were then incubated at 30 –37 °C for 4 – 7 days. The lowest concentration that did not show growth of the test organisms was considered to be [33].

 ISSN: Online 2790-1637, Print 2790-1629
National Library of Libya, Legal number: 154/2018

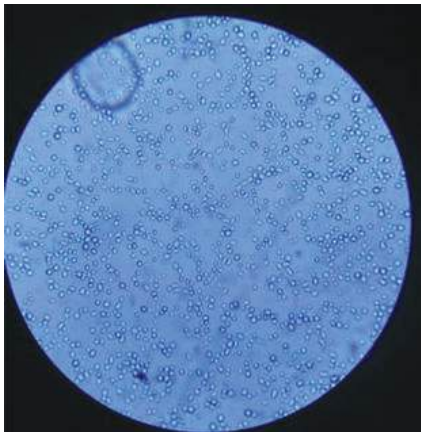

Figure. 1. Shows the C. albicans shape of the microscopic diagnosis.

Figure. 2. Shows the growth C. albicans on the media.

3.RESULTS AND DISCUSSION

Bonferroni test was used for statistical analysis to show if there any significant difference ($P \leq 0.05$).

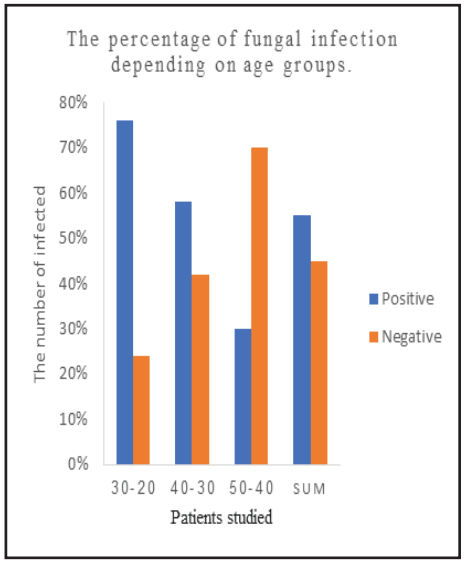

Figure.3. Shows the number of patients studied, the number of infected and healthy plates, and the percentage of fungal infection depending on age groups.

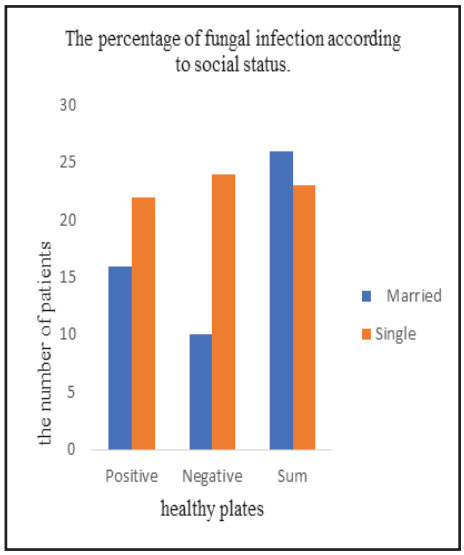

Figure.4. Shows the number of patients studied, the number of infected and healthy plates, and the percentage of fungal infection according to social status.

 ISSN: Online 2790-1637, Print 2790-1629
National Library of Libya, Legal number: 154/2018

Table 1. Evaluations of the antifungal potential of the aquatic extract of plants Allium sativm, salvia rosmarinus and Mentha used.

Microorganism	**Concentration 100%**		
Fungi	Inhibition zone (mm)		
C. albicans	Allium sativum	Salvia rosmarinus	Mentha
Men inhibition zone(mm)	1.41	0.72	-

Table 2. Minimum inhibitory and bactericidal concentrations of aquatic extract of propolis against fungi .

Isolation	**fungal strain with inoculums density of 10^8CFU/m**	**Antimicrobial activity of Plant% (V/V)**			
		Allium sativm extract		**Salvia rosmarinus extract**	
		MIC	MBC	MIC	MBC
Vagiana	C. albicanas	2:4	2:2	2:2	-

After isolating the fungus from some patients attending Awjila Al-Qarawi Hospital and the Red Crescent Clinic in Jalu, the results are shown in Fig.3, for the period from April to July. Approximately 72 cases were studied, all of which underwent laboratory treatment, from the beginning of the sample culture on sabouraud dextrose medium until the end of the test. It was found that the number of positive results was highest among young people aged 20-30, while it decreased slightly among adults aged 30 - 40, and decreased by half between the ages of 40-50, as the table shows. This difference in infection rates among patients despite the fact that they all suffer from the same or nearly similar symptoms is explained by the fact that as people age, their cells become more resistant to the C. fungus, and the immune system strengthens and becomes more capable of fighting off infection, despite the fact that some cases are infected with bacteria whose symptoms are somewhat similar to those of C. fungi. Therefore, treatment is usually administered in some cases as a dual therapy consisting of doses of antibiotics that combat bacterial growth and those that combat fungal growth simultaneously, of the 72 samples, 42 % (31 samples) tested positive for Candida, while 57 % (41 samples) tested negative or tested for other microbial species. The results indicate that vulvovaginal candidiasis is widespread among women in the study area. This is consistent with a previous study conducted in North Africa (2022) [34], which showed an incidence rate ranging from 15-52 % depending on the region and diagnostic method. The results showed the highest infection rate (62.3 % of positive cases) in women aged 20-30 years. The study showed that women of this age group, which is considered reproductive age, are more susceptible to infection. This is consistent with a study conducted in 2022 [35], which recorded the highest infection rates among this group. This is attributed to hormonal changes, increased sexual activity, pregnancy, and the use of hormonal contraceptives. While the infection rate reached 29 % for the age group (30-40), the lowest infection rate was 9.7% for the age group above (40). This was evident in the decrease in infection with age due to the decline in estrogen levels after menopause. The study, in Fig.4, shows the distribution of infection by marital status, with 26 cases in the married group, of which 16 were positive (22.02 %), and 10 were negative. Forty-six samples were collected from the unmarried group, and the results showed that 22 samples were positive (30.5 %) out of 24 samples that were negative. The presence of infection in both groups is evidence of the presence of factors associated with infection, such as a humid environment, wearing tight clothing, vaginal microbial imbalance, the use of vaginal douching, as well as the excessive use of antibiotics, diabetes, and contraceptives [36].

 ISSN: Online 2790-1637, Print 2790-1629
National Library of Libya, Legal number: 154/2018

3.1. Evaluations of the antifungal potential of the Aquatic extract of plants Allium sativm, Salvia rosmarinus and Mentha used . Use of Salvia rosmarinus and mint(Mentha) extracts:

3.1.1.Effect of the aqueous extract on fungi isolated from the vagina:

Among the available methods for testing antifungal activity, the disk diffusion method (measurable inhibition zones) was used to determine the effectiveness of the aqueous extract against a single species of human-pathogenic fungi [37].

Table 1. Shows the results of tests of the antifungal activity of a 100 % v/v aqueous extract sample on fungi isolated from the vagina. The results showed that the fungal isolates obtained from the patients were C. albicans. This was confirmed by several methods, including the morphological description of the fungus or the general shape of the fungal colonies, which was confirmed by comparing the isolate we obtained with isolates identified in local research centers. We did not limit ourselves to morphology alone. All isolates were examined under a light microscope, and samples were sent to mycologists to confirm that they were the exact fungus. The isolates were also compared in terms of their morphology and microscopic appearance with previous studies on Candida fungi (C. fungi), and all data obtained were consistent with these studies. It became clear that the general "phenotypic" and microscopic appearance of the fungus was consistent with these studies. These are as follows: In terms of the fungus's physical appearance, it appears on nutrient media as white to pale yellow colonies with a waxy sheen. Colonies initially form on nutrient media in the form of circles that overlap with each other as the colony grows. Under the microscope, the fungus appears as oval cells, very similar in shape and reproduction to the yeast saccharomyces ceriveciae. Fungi are unicellular and reproduce by budding. They differ from yeast in that they are imperfect fungi, while yeast is a cyst-shaped fungus at 37 °C and a pseudofungi at 25-27 °C.

To determine the antifungal effect of Allium sativum, Salvia rosmarinus, and Mentha extracts on the growth and inhibition of C. fungi, it was found by monitoring dishes containing 15 tablets impregnated with plant extracts (Allium sativum, Salvia rosmarinus, and Mentha) five tablets per dish out of a total of three that during the first three days, no change in fungal growth was observed. However, after three days, slow fungal growth was observed toward the disc impregnated with either Mentha or Ocimum basilicum extract. The fungus continued to grow very slowly but did not directly reach the disc. The results showed significant inhibition of Allium sativum extract, with an average inhibition zone ranging from 1-2 mm, with an average inhibition zone of 1.44 mm in diameter. The results of Salvia rosmarinus extract showed a moderate inhibition zone, ranging from 0.6-1 mm, with an average inhibition zone of 9.89 mm in diameter. Mentha extract showed no inhibition zone at all. The reason for the low or absent inhibitory effectiveness of the studied plant extracts may be due to the presence of the plant extracts themselves in the fungal growth medium. These extracts may contain compounds that inhibit or inhibit the growth of some microorganisms, but some may lose their inhibitory capacity during extraction or storage. The method of preparing the plant extracts and their concentration are two important factors. This may be due to the nature of the extracts themselves. They may contain compounds that inhibit or inhibit the growth of some microorganisms, but some may lose their inhibitory capacity during extraction or storage [38].

3.2. Minimum inhibitory concentration (MIC) and minimum bactericidal concentration (MBC)

The minimum inhibitory concentration (MIC) and minimum bactericidal concentration (MBC) for extracts aquatic were assessed on fungal strain for control and comparison purposes and was the result obtained showed in Table 2.

4.CONCLUSION

After isolating the fungus C. albicans from clinical samples in the oases area, three plant extracts were tested for their ability to inhibit the growth of C. albicans using

 ISSN: Online 2790-1637, Print 2790-1629
National Library of Libya, Legal number: 154/2018

standard laboratory tests. The plant extracts extracted from medicinal plants were Allium sativum, Salvia rosmarinus, and Mentha. Both Allium sativum, Salvia rosmarinus gave good and very similar results in terms of fungal inhibition, except for Mentha extract, which did not produce encouraging results in inhibiting C. albicans. This suggested that the compounds found in Allium sativum, Salvia rosmarinus may offer a valuable alternative or complement to antifungal treatments, especially for C. albicans. The method of preparation of the plant extracts, their concentration, storage method, and the duration of their extraction are important factors that affect the inhibition process.

REFERENCES

1.Macias-Paz, I. U., Pérez-Hernández, S., Tavera-Tapia, A., Luna-Arias, J. P., Guerra-Cárdenas, J. E., & Reyna-Beltrán, E. (2023). Candida albicans the main opportunistic pathogenic fungus in humans. Revista Argentina de microbiología, 55(2), 189-198. https:// doi.org/10.1016/j.ram.2022.08.003

2.Duan, Y., Wang, Z. J., Mei, L. N., Shen, J. S., He, X. C., & Luo, X. D. (2025). Anti-Candida albicans effect and mechanism of Pachysandra axillaris Franch. Journal of Ethnopharmacology, 340, 119284. https://doi.org/10.1016/j.jep.2024.119284

3.Rocha, F. M. G., Rocha, C. H. L., Silva, L. C. N., Pinheiro, A. J. M. C. R., Mendonca, A. M. S., Cantanhede Filho, A. J., ... & Monteiro, C. A. (2025). n-butanol fraction of Terminalia catappa possesses anti-Candida albicans properties and in vivo action on Tenebrio molitor alternative infection model. Microbial Pathogenesis, 198, 107133. https: //doi.org/10.1016/j.micpath.2024.107133

4.Cordisco, E., Petenatti, E., Svetaz, L., & Sortino, M. (2021). Evaluation of the antifungal photodynamic activity of Thymophylla pentachaeta extracts against Candida albicans and its virulence factors. Phytomedicine, 90, 153608. https: //doi.org/ 10.1016/ j.phymed. 2021. 153608

5.Serrano, A., Basante-Bedoya, M. A., Bassilana, M., & Arkowitz, R. A. (2023). A live-cell ergosterol reporter for visualization of the effects of fluconazole on the human fungal pathogen Candida albicans. Mbio, 14(6), e02493-23. https://doi.org/10.1128/mbio.02493-23

6.MacAlpine, J., Liu, Z., Hossain, S., Whitesell, L., Robbins, N., & Cowen, L. E. (2023). DYRK-family kinases regulate Candida albicans morphogenesis and virulence through the Ras1/PKA pathway. MBio, 14(6), e02183-23. https://doi.org/10.1128/mbio.02183-23

7.Iyer, K. R., Robbins, N., & Cowen, L. E. (2022). The role of Candida albicans stress response pathways in antifungal tolerance and resistance. Iscience, 25(3). https://doi.org/10.1016/j.isci. 2022.103953

8.Robbins, N., & Cowen, L. E. (2023). Roles of Hsp90 in Candida albicans morphogenesis and virulence. Current opinion in microbiology, 75, 102351. https: //doi.org/10.1016/ j.mib. 2023.102351

9.Li, L., Lu, H., Zhang, X., Whiteway, M., Wu, H., Tan, S., ... & Jiang, Y. (2022). Baicalein acts against Candida albicans by targeting Eno1 and inhibiting glycolysis. Microbiology spectrum, 10(4), e02085-22. https://doi.org/10.1128/spectrum.02085-22

10.Murdoch, L. E., McKenzie, K., Maclean, M., Macgregor, S. J., & Anderson, J. G. (2013). Lethal effects of high-intensity violet 405-nm light on Saccharomyces cerevisiae, Candida albicans, and on dormant and germinating spores of Aspergillus niger. Fungal Biology, 117(7-8), 519-527. https://doi.org/10.1016/j.funbio.2013.05.004

11.Yang, F., Gritsenko, V., Slor Futterman, Y., Gao, L., Zhen, C., Lu, H., ... & Berman, J. (2021). Tunicamycin potentiates antifungal drug tolerance via aneuploidy in Candida albicans. MBio, 12(4), 10-1128. https://doi.org/10.1128/mbio.02272-21

12.[Mu, C., Pan, C., Han, Q., Liu, Q., Wang, Y., & Sang, J. (2019). Phosphatidate phosphatase Pah1 has a role in the hyphal growth and virulence of Candida albicans. Fungal Genetics and Biology, 124, 47-58. https://doi.org/10.1016/j.fgb.2018.12.010

13.Kiliszek, A., Rypniewski, W., Rząd, K., Milewski, S., & Gabriel, I. (2019). Crystal structures of amino-

transferases Aro8 and Aro9 from Candida albicans and structural insights into their properties. Journal of Structural Biology, 205(3), 26-33. https: //doi.org/ 10.1016/j.jsb.2019.02.001

14.Yu, T., Hou, J., Hafeez, F., Ge, P., Zou, A., Fu, Y., ... & Xianyu, Y. (2024). Fungus-mediated biosynthesis of gold nanoparticles with synergistic antifungal activity against multidrug-resistant Candida albicans. Nano Today, 59, 102486. https: //doi.org/ 10.1016/ j.nantod.2024.102486

15.Rahmatian, N., Abbasi, S., Abbasi, N., & Yaraki, M. T. (2024). Alginatecarbon dot nanocomposite: A green approach towards designing turn-on aptasenor for Candida albicans fungus. International Journal of Biological Macromolecules, 282, 137315. https: //doi.org/10.1016/j.ijbiomac.2024.137315

16.Holzknecht, J., Dubrac, S., Hedtrich, S., Galgóczy, L., & Marx, F. (2022). Small, cationic antifungal proteins from filamentous fungi inhibit Candida albicans growth in 3D skin infection models. Microbiology Spectrum, 10(3), e00299-22. https: //doi.org/ 10.1128/ spectrum. 00299-22

17.Arasu, A., Pingley, V., Prabha, N., OV, R., Annathurai, K., Kasirajan, S., ... & Arockiaraj, J. (2021). Impact and fungitoxic spectrum of Trachyspermum ammi against Candida albicans, an opportunistic pathogenic fungus commonly found in human gut that causes Candidiasis infection. Journal of Infection and Public Health, 14(12), 1854-1863. https: //doi.org/ 10.1016/j.jiph.2021.09.027

18.Yin, W., Zhang, Y., Cui, H., Jiang, H., Liu, L., Zheng, Y., ... & Cheng, M. (2021). Design, synthesis and evaluation of novel 5-phenylthiophene derivatives as potent fungicidal of Candida albicans and antifungal reagents of fluconazole-resistant fungi. European Journal of Medicinal Chemistry, 225, 113740. https://doi.org/10.1016/j.ejmech.2021.113740

19.Chatterjee, S., Ghosh, R., & Mandal, N. C. (2020). Inhibition of biofilm-and hyphal-development, two virulent features of Candida albicans by secondary metabolites of an endophytic fungus Alternaria tenuissima having broad spectrum antifungal potential. Microbiological research, 232, 126386. https: //doi.org/ 10.1016/j.micres. 2019. 126386

20.Van Genechten, W., Demuyser, L., Duwé, S., Vandenberg, W., Van Dijck, P., & Dedecker, P. (2021). Photochromic fluorophores enable imaging of lowly expressed proteins in the autofluorescent fungus Candida albicans. Msphere, 6(2), 10-1128. https: //doi.org/ 10.1128/msphere.00146-21

21.Vilela, C., Oliveira, H., Almeida, A., Silvestre, A. J., & Freire, C. S. (2019). Nanocellulose-based antifungal nanocomposites against the polymorphic fungus Candida albicans. Carbohydrate Polymers, 217, 207-216. https: //doi.org/ 10.1016/ j.carbpol. 2019. 04. 046

22.Belghit, S., Driche, E. H., Bijani, C., Zitouni, A., Sabaou, N., Badji, B., & Mathieu, F. (2016). Activity of 2, 4-Di-tert-butylphenol produced by a strain of Streptomyces mutabilis isolated from a Saharan soil against Candida albicans and other pathogenic fungi. Journal de mycologie medicale, 26(2), 160-169. https://doi.org/10.1016/j.mycmed.2016.03.001

23.Djihane, B., Wafa, N., Elkhamssa, S., Pedro, D. H. J., Maria, A. E., & Mihoub, Z. M. (2017). Chemical constituents of Helichrysum italicum (Roth) G. Don essential oil and their antimicrobial activity against Gram-positive and Gram-negative bacteria, filamentous fungi and Candida albicans. Saudi Pharmaceutical Journal, 25(5), 780-787. https: //doi.org/ 10.1016/j.jsps.2016.11.001

24.Kniemeyer, O., Schmidt, A. D., Voedisch, M., Wartenberg, D., & Brakhage, A. A. (2011). Identification of virulence determinants of the human pathogenic fungi Aspergillus fumigatus and Candida albicans by proteomics. International Journal of Medical Microbiology, 301(5),368-377. https://doi.org/10.1016/j.ijmm.2011.04.001

25.Moradkhah, S., Larypoor, M., & Allahverdi, A. (2025). Design and Fabrication of a Rapid Detection Biosensor for Candida albicans Diagnosis in a Microfluidic Platform. Talanta Open, 100478. https://doi.org/10.1016/j.talo.2025.100478

26.Isbilir, H., Kaya, H. O., Tekintaş, Y., Kurul, F., Cetin,

 ISSN: Online 2790-1637, Print 2790-1629
National Library of Libya, Legal number: 154/2018

A. E., & Topkaya, S. N. (2025). Enhanced electrochemical biosensing of Candida albicans via $NiFe_2O_4$ nanoparticle-doped imprinted polymers. Microchemical Journal, 114513. https: //doi.org/ 10.1016/ j.microc. 2025.114513

27.Liu, R., Ji, W., Jiang, M., & Shen, J. (2025). CRISPR technology combined with isothermal amplification methods for the diagnosis of Candida albicans infection. Clinica Chimica Acta, 567, 120106. https://doi.org/10.1016/j.cca.2024.120106

28.Yue, D., Zheng, D., Yang, L., Bai, Y., Song, Z., Li, D., ... & Li, Y. (2025). Berberine disrupts the high-affinity iron transport system to reverse the fluconazole-resistance in Candida albicans. Microbial Pathogenesis, 200, 107370. https: //doi.org/ 10.1016/ j.micpath.2025.107370

29.Ko, B. S., Park, S. G., & Rhee, M. S. (2025). Synergistic antifungal effect of naturally-derived antimicrobials with penetration enhancer against Candida albicans biofilm at 5° C and 22° C. Journal of Infection and Public Health, 102882. https: //doi.org/ 10.1016/j.jiph.2025.102882

30.Ordiales, H., Olano, C., Martín, C., Blanco-Agudín, N., Alcalde, I., Merayo-Lloves, J., & Quirós, L. M. (2025). Phosphoglycerate mutase and methionine synthase act as adhesins of Candida albicans to the corneal epithelium, altering their expression during the tissue adhesion process. Experimental Eye Research, 254, 110322. https: //doi.org/ 10.1016/j.exer.2025.110322

31.Rivera, A., Viñado, B., Benito, N., Docobo-Pérez, F., Fernández-Cuenca, F., Fernández-Domínguez, J., ... & Navarro, F. (2023). Recommendations of the Spanish Antibiogram Committee (COESANT) for in vitro susceptibility testing of antimicrobial agents by disk diffusion. Enfermedades Infecciosas y Microbiología Clínica, 41(9), 571-576. https: //doi.org/ 10.1016/j.eimce.2022.12.009

32.Wilson, D. (2019). Candida albicans. Trends in Microbiology, 27(2), 188-189. https: //doi.org/ 10.1016/j.bbagen.2014.03.014

33.Favre, B., Hofbauer, B., Hildering, K. S., & Ryder, N. S. (2003). Comparison of in vitro activities of 17 antifungal drugs against a panel of 20 dermatophytes by using a microdilution assay. Journal of clinical microbiology, 41(10), 4817-4819. doi: 10.1128/JCM.41.10.4817-4819.2003

34.Jabri, B., Iken, M., Ait-Ou-Amar, S., Rida, S., Bouziane, A., & Ennibi, O. K. (2022). Candida albicans and Candida dubliniensis in periodontitis in adolescents and young adults. International Journal of Microbiology, 2022(1), 4625368. https: //doi.org/10.1155/2022/4625368

35.Mohamed, A. O., Mohamed, M. S., Mallhi, T. H., Hussain, M. A., Jalloh, M. A., Omar, K. A., ... & Ali, A. A. M. M. (2022). Prevalence of vulvovaginal candidiasis among pregnant women in Africa: A systematic review and meta-analysis. The Journal of Infection in Developing Countries, 16(08), 1243-1251. doi:10.3855/jidc.15536

36.Payne, V. K., Florence Cécile, T. T., Cedric, Y., Christelle Nadia, N. A., & José, O. (2020). Risk factors associated with prevalence of Candida albicans, Gardnerella vaginalis, and Trichomonas vaginalis among women at the district hospital of Dschang, west region, Cameroon. International Journal of Microbiology, 2020(1), 8841709. https: //doi.org/ 10.1155/2020/8841709

37.Ōsuke, M. (1959). Fundamental study on the disc method of antibiotic sensitivity test. The Journal of Antibiotics, Series A, 12(5), 263-284. https: //doi.org/10.11554/ antibioticsa. 12.5_263

38.Mdee, L. K., Masoko, P., & Eloff, J. N. (2009). The activity of extracts of seven common invasive plant species on fungal phytopathogens. South African Journal of Botany, 75(2), 375-379. https://doi.org/10.1016/j.sajb.2009.02.003

Scientific Journal of University of Benghazi

SJUOB (2025) 38 (2) Applied Sciences: Elshibani. & Abdalkader, 43 – 55
www.sjuob.uob.edu.ly

Mechanical and Microstructural Proxies of LC³ Mortars up to 50% Clinker Replacement Using a Southern Libyan Calcined Kaolinite Clay.

Zainab M. Elshibani[1], Ashraf H. Abdalkader[1]*.

1.Department of Civil Engineering, University of Benghazi, Libya.

DOI: 10.37376/sjuob.v38i2 | Received:24/08/2025 | Accepted:17/10/2025 | Publishing: 23/12/2025

ABSTRACT

This experimental study investigates the properties of LC³ (limestone-calcined clay) cement mortars with high clinker replacement, utilizing locally sourced kaolinite-rich clays from southern Libya. Mortar mixtures were prepared with clinker contents of 40, 50, and 60%. The mechanical performance of the LC³ blends was assessed through compressive and flexural strength tests, ultrasonic pulse velocity (UPV), porosity measurements, and workability evaluations. The results show that replacing up to 50% of cement with a limestone–calcined clay blend in mortar mixes achieves compressive and flexural strengths comparable to, or slightly exceeding, those of ordinary cement. At 28 days, mortars with 50% substitution reached the same compressive strength as CEM I (37 MPa) while exhibiting a 19.6% increase in flexural strength. Furthermore, higher replacement levels (up to 50%) improved pore structure refinement, leading to a denser microstructure. Mortars with 50% substitution demonstrated about a 9.65% reduction in porosity compared to CEM I.

KEYWORDS: LC³ blends cement, Clinker replacement, Compressive strength, Flexural strength, Workability, Porosity.

Corresponding Author: Ashraf H. Abdalkader, ashraf.abdalkader@uob.edu.ly

 ISSN: Online 2790-1637, Print 2790-1629
National Library of Libya, Legal number: 154/2018

1.INTRODUCTION

Metakaolin (MK), a highly reactive pozzolanic material, enhances both early-age strength and long-term durability in cementitious systems by refining their pore structure (Sabir et al., 2001). To reduce the high clinker content in conventional cement, supplementary cementitious materials (SCMs) are commonly employed; however, replacing more than 30% of clinker often reduces early strength. Given the limited availability of industrial by-product SCMs such as fly ash and slag, calcined clays rich in kaolinite have emerged as promising alternatives due to their ability to form reactive metakaolin upon thermal activation (Antoni et al., 2012) . Limestone calcined clay cement (LC^3), introduced in 2012, offers a sustainable solution by combining calcined clay (CC) and limestone (LS), enabling clinker replacement levels of up to 60% through the synergistic pozzolanic reaction between alumina and carbonates (Antoni et al., 2012). In addition to its technical performance, LC^3 aligns with circular economy principles by lowering CO_2 emissions and encouraging the utilization of abundant and low-cost raw materials. As the construction industry increasingly prioritizes sustainability, research has turned toward optimizing low-carbon binder systems through tailored mix design and a deeper understanding of hydration and reaction mechanisms (Snellings, 2016). Research by Hawkins et al., (2003) has shown that incorporating up to 5% limestone in ordinary Portland cement (OPC) does not compromise strength and improves energy efficiency by enhancing the grinding process. Moreover, when combined with calcined clay, limestone enhances the performance of ternary blends by participating in additional reactions (Dhandapani et al., 2021).

In the Libyan context, the industrial research centre has identified large deposits of kaolinite-rich clay in the southern region, which can be thermally activated at 700–850 °C to produce reactive metakaolin (Akasha, 2015). These local resources present a strategic opportunity to develop sustainable cementitious systems within the region. The performance of LC^3 is influenced by several interrelated factors, including the purity and mineralogical composition of raw materials, the calcination temperature, curing conditions, and overall mix design. Key parameters such as the grinding sequence, gypsum content, water-to-binder ratio, CC-to-LS ratio, and the clinker replacement level have been shown to significantly affect both mechanical strength and workability (Balasubramanian & Sarangapani, 2023). Previous studies (Lin et al., 2021, Yu et al., 2021, Balasubramanian and Sarangapani, 2023) have highlighted the sensitivity of compressive strength to these variables. Lin et al. (2021) reported that a mix composed 85% OPC, 10% calcined clay, and 5% limestone yielded the highest compressive strength, with further increases in substitution leading to a decline in performance. Likewise, Yu et al. (2021) showed that LC^3 blends with 50-70% clinker content complied with BS EN 197-1 strength standards. Balasubramanian and Sarangapani (2023) further supported these findings, noting that clinker replacement levels could vary between 30 and 70%, contingent on the quality and purity of the supplementary materials used. Kafodya et al., (2023) evaluated LC3 cement made with local Malawian materials at two clinker levels: 50% (LC3-50) and 40% (LC3-40). Using varying calcined clay-to-limestone ratios and water-to-cement ratios, results showed that LC3-50 achieved higher compressive strength (up to 39.2 MPa) at 28 days. Increased clay content reduced workability and strength due to higher water demand. LC3-50 also showed lower porosity and improved microstructure, confirming its potential as a sustainable cement alternative. Chaipanich et al., (2024) examined the replacement of 50% of OPC with varying proportions of limestone (30 - 45%) and calcined clay (5 - 20%). Their findings showed that the optimal blend (30% LS, 20% CC) achieved a compressive strength of 36 MPa at 28 days 225% higher than the blend containing 50% limestone only. The improved performance was attributed to the enhanced pozzolanic reactivity and improved pore structure associated with higher CC content. Although the strength remained below that of 100%

OPC, the blend demonstrated promising performance for use as a low - carbon, medium - strength alternative binder. Nararueang et al., (2024) explored the performance of various Thai calcined clays as partial replacements for OPC across six different mixtures containing fly ash (FA), MK, and regional CCs. Despite identical clinker replacement levels across the blends, those incorporating calcined clays outperformed fly ash-based mixes in terms of both compressive strength and ultrasonic pulse velocity (UPV). These improvements were attributed to the higher pozzolanic activity of calcined clays, which resulted in lower porosity and better mechanical performance. Ferrari et al., (2023) investigated how increasing CC content affects mortar workability through flow table tests performed on both mortars and pastes at water-to-binder (w/b) ratios of 0.5 and 0.4, using CEM-I and CEM-II cements. Their findings confirmed that higher CC contents significantly reduce workability due to rapid water absorption by CC, which reduces the amount of free water available for paste fluidity. This behavior necessitated greater use of superplasticizers to maintain adequate workability. Complementary to this, Takhi et al., (2024) examined the fresh properties of LC³ systems with 50 and 70% clinker replacement, employing different CC:LS ratios (2:1 and 1:1). Compared to OPC, these mixes exhibited increased water demand and prolonged setting times with higher CC content. The reduced flowability was once again linked to the water-retaining nature of metakaolin, which imposes a need for higher superplasticizer dosages to achieve workability comparable to OPC. Shao et al., (2025) further reported that although LC³ tends to have slightly lower compressive strength than OPC at early ages, it typically matches or surpasses OPC by 7 days, with continued strength development through 28 days. This trend consistent across multiple studies demonstrates that LC³ can achieve comparable long-term mechanical performance with substantially lower clinker content. Furthermore, LC³ concrete has exhibited superior flexural strength and enhanced chloride-binding capacity, broadening its applicability in durable construction. Despite these advances, research is still limited on the effects of high clinker replacement levels (≥50%) on the performance of LC³. In particular, no previous studies have investigated high clinker replacement LC³ produced with kaolinite-rich clays from Libya.

This experimental study examines the properties of LC³ (limestone-calcined clay) cement mortars featuring high clinker replacement levels, incorporating locally sourced kaolinite-rich clays from southern Libya. Mortar mixtures were formulated with clinker contents of 40, 50, and 60%. The performance of the LC³ blends was evaluated through compressive strength tests, flexural strength tests, ultrasonic pulse velocity (UPV) measurements, porosity analysis, and workability assessments.

2.EXPERIMENTAL WORK

2.1.Materials:

Portland cement CEM-I 42.5 N, sourced from the Benghazi Cement Factory, was used in this study. This cement meets the European standard (EN 197-1, 2011). The limestone was also procured from the same factory, where it was dried, ground, and sieved to pass through a 75 µm sieve. Gypsum, provided by the cement factory, was milled and sieved to achieve a particle size of less than 75 µm. The chemical and physical characteristics of the cement, limestone, and gypsum are summarized in Tables 1, while Figure 1 illustrates the limestone and gypsum before and after grinding.

 ISSN: Online 2790-1637, Print 2790-1629
National Library of Libya, Legal number: 154/2018

Table 1. Properties of cement, limestone, and gypsum.

Chemical Composition (%)	Cement	Limestone	Gypsum
CaO	62.62	52.00	51.92
SiO_2	20.65	1.65	1.74
Al_2O_3	5.17	0.34	1.20
Fe_2O_3	2.77	0.04	0.14
MgO	3.33	2.16	1.06
Na_2O	-	-	3.95
K_2O	-	0.09	0.13
Cl	-	0.05	-
SO_3	2.61	0.58	39.28
LOI	1.56	44.97	32.81
Surface area (Blaine) m^2/kg	360	-	-
Finesses (%)	3.23	-	-

Figure 1. Finely milled limestone and gypsum.

Standard sand, sourced from the Benghazi Cement Factory, met the specifications outlined in (ASTM778, 2009) was used to prepare the mortar specimens. Kaolinite-rich clays were sourced from 10 km north of Sebha in southern Libya, comprising about 95% kaolinite. This clay is classified as type A (Akasha, 2015). The raw clay was crushed into fragments ranging from 0.5 to 1.25 cm and then calcined at 800 °C for two hours in a controlled furnace (type 30400, see Figure 2). After calcination, the materials were cooled in an airtight desiccator to maintain their reactivity. The resulting calcined clays were processed using a Los Angeles abrasion machine, then a conventional mill, and finally sieved to ensure they passed through a 75 µm sieve, as shown in Figure 3. The chemical composition of the calcined clays is detailed in Table 2.

Figure 2. Type 30400 furnace used.

Figure 3. Finely milled calcined clay

Table 2. The chemical analysis of calcined clay (by XRF).

Chemical composition (%)	Sebha clay type (A)
SiO_2 56.14	
Al_2O_3	32.74
Fe_2O_3	2.41
CaO	6.86
CI	0.16
Na_2O	0.6
K_2O	-

 ISSN: Online 2790-1637, Print 2790-1629
National Library of Libya, Legal number: 154/2018

Chemical composition (%)	Sebha clay type (A)
SO_3	-
TiO_2	-
MnO	0.01
P_2O_5	0.07

2.2.Mixture Details:

A total of four mortar mixtures (Table 3) were designed to evaluate the influence of combined calcined clay (CC) and limestone (LS), at a fixed ratio of 2:1, on the mechanical performance of blended cement mortars. To mitigate the potential impact of sulfate interaction, the gypsum (Gyp) content was maintained at 6% in all mixtures. This approach aligns with established practices for maintaining the balance between setting time and strength development in cementitious systems, as sulfate levels can significantly influence hydration kinetics and ettringite formation (Taylor, 1997). Three LC^3-based mixes were prepared with clinker contents of 60, 50, and 40%. Each of these mixes contained 6% gypsum, with the remaining fraction composed of calcined clay (CC) and limestone (LS) at the 2:1 ratio. Additionally, control mixture was included using CEM I 42.5 with no substitution of calcined clay or limestone. The detailed composition of all mixtures is presented in Table 3, and the obtained LC^3 blends cement mixtures are given in Figure 4.

Table 3. System compositions.

Mixture ID	Clinker(%)	CC(%)	LS(%)	Gypsum(%)	Total(%)	Clinker Reduction vs CEM	CC:LL Ratio
CEM	94.00	-	-	6	100	-	-
LC^3-60	60.00	22.67	11.33	6	100	36.17	2:1
LC^3-50	50.00	29.33	14.67	6	100	46.81	2:1
LC^3-40	40.00	36.00	18.00	6	100	57.45	2:1

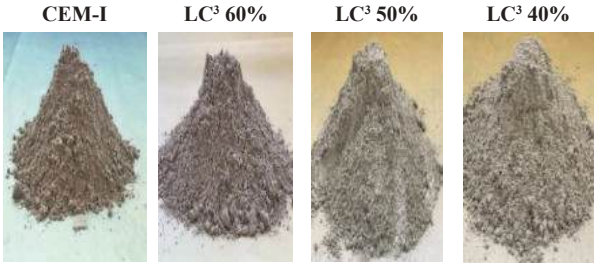

Figure 4. LC^3 blends cement mixtures.

2.3.Specimens Preparation:

Mortar mixtures were prepared for 50 mm cubes (following ASTM C109/C109M-02, 2020) and 40 × 40 × 160 mm prisms (per ASTM C348-21, 2021) to assess compressive and flexural strength, respectively. In all mixtures, a water-to-binder ratio of 0.485 and a binder-to-sand ratio of 1:2.75 (by weight) were adopted. The control mixture (CEM) was prepared with a water-to-cement ratio (w/c) of 0.485, in accordance with ASTM C109, to achieve a target mortar flow of 110 ± 5% on the flow table. For all other mixtures, the water-to-binder ratio (w/b) was consistently maintained at 0.485 as a controlled variable. As a result, the measured flow values differed based on the clinker replacement level in each formulation. Notably, no superplasticizer (SP) was needed to achieve the desired workability. Mixing was conducted with an automatic mortar mixer in compliance with (ASTM C305/C305-20, 2009). The mortar specimens were compacted, kept in molds for 24 hours, demolded, and then cured in water until testing.

2.4.Test Methods:

The hardened densities of cement mortars were measured in compliance with ASTM C188. Workability was assessed using the flow table test (ASTM C1437, 2007).

 ISSN: Online 2790-1637, Print 2790-1629
National Library of Libya, Legal number: 154/2018

Compressive strength was determined at different curing ages (3, 7, 28, 56 days) using 50 mm mortar cubes, following ASTM C109. Flexural strength was evaluated after 28 days using 40 × 40 × 160 mm mortar prisms as per ASTM C348-21.

Porosity was evaluated at 3, 7, and 28 days using 50 mm mortar cubes following the vacuum saturation procedure described in RILEM (1994). The open porosity of the samples was determined in accordance with RILEM Recommendation CPC 11.3, which quantifies the volume of accessible pores through vacuum saturation and subsequent mass measurements of the specimens in dry, saturated, and immersed conditions. Prior to testing, mortar samples were oven-dried at 105 ± 5 °C until a constant mass was achieved, then cooled to room temperature in a desiccator. Vacuum saturation was carried out as per CPC 11.3: a vacuum pressure of ≤ 2 kPa was maintained for 3 hours to evacuate air from the open pores. Deionized water was then gradually introduced under vacuum for an additional 1 hour to ensure full infiltration. All procedures were performed at 20 ± 2 °C to minimize temperature-related changes in water viscosity and specimen stability. After vacuum release, specimens remained fully submerged in water for 24 hours to achieve complete saturation. Three masses were subsequently recorded: the dry mass (Md) after oven drying, the saturated-surface-dry mass (Ms) after vacuum saturation and gentle blotting, and the immersed mass (Mi) while suspended in water. The accessible porosity (P) was then calculated using equation (2.4.1) below:

$$P = \left[\frac{Ms - Md}{Ms - Mi}\right] x100 \qquad (2.4.1)$$

Additionally, the ultrasonic pulse velocity (UPV) was measured on 50 mm mortar cubes at different curing ages following the procedure outlined in ASTM C597-09 (2010). The test was conducted to assess the quality, uniformity, and internal condition of the mortar specimens. A pulse velocity apparatus equipped with 54 kHz transducers was employed for all measurements. To ensure efficient signal transmission, a thin film of gel was applied between the transducers and the opposite faces of each specimen. Prior to testing, the mortar cubes were conditioned to a saturated-surface-dry (SSD) state. This state was achieved by immersing the cubes in water for 24 hours, followed by gentle wiping of any surface moisture immediately before the test. All UPV measurements were carried out at a controlled laboratory temperature of 20 ± 2 °C. The pulse velocity (V) was calculated using the equation (2.4.2) below:

$$V = \frac{L}{t} \qquad (2.4.2)$$

where L represents the travel path length (Km) and t denotes the measured travel time (s).

The reported values of compressive strength, flexural strength, and porosity represent the averages of 3, 2, and 1 test specimens per age, respectively.

3.RESULTS AND DISCUSSION

3.1.Density of Hardened Mortar:

Figure 5 shows a comparison of density among different types of LC^3 blends cement mortars. CEM has the highest density, while LC^3-40 has the lowest. The densities of LC^3-60 and LC^3-50 fall between these two, with LC^3-60 being denser than LC^3-50. This suggests that as the LC^3 blend ratio changes, the density of the mortar decreases.

 ISSN: Online 2790-1637, Print 2790-1629
National Library of Libya, Legal number: 154/2018

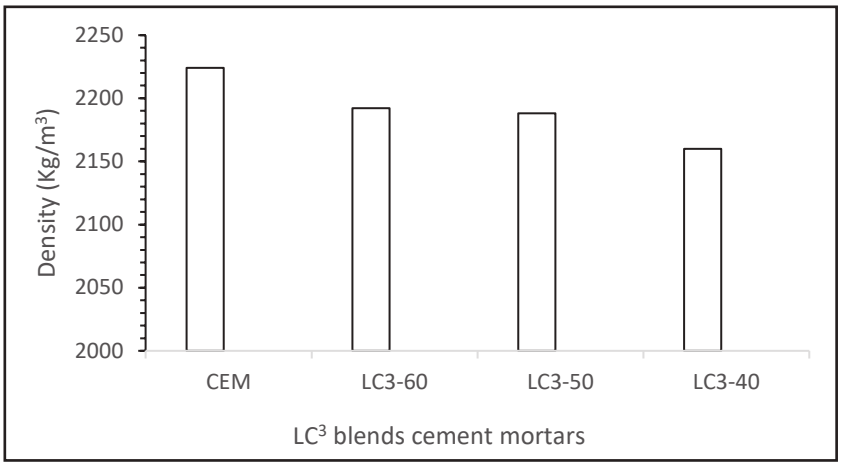

Figure 5. Hardened density of LC³ blends cement mortars.

3.2.Workability:

The results of mortar's flow are shown in Figure 6. It can be seen from the graph that workability declins with rising replacement levels, highlighting a trade-off between sustainability and fresh-state performance, consistent with findings by (Balasubramanian & Sarangapani, 2024).

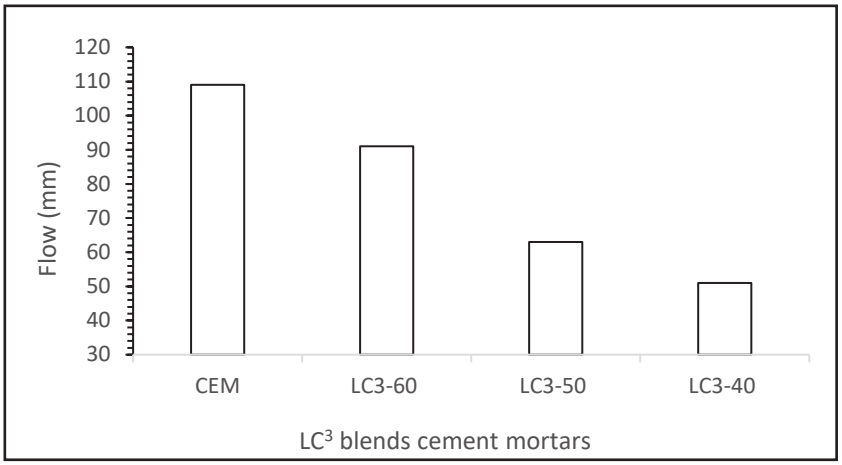

Figure 6. Flow of LC³ blends cement mortars.

3.3.Compressive Strength:

The results of compressive strength of CEM I and LC³ blends cement mortars are shown in Figure 7. All mortars gain strength with age, showing the expected trend of increasing compressive strength as hydration progresses. LC3-60 consistently demonstrates the highest compressive strength at all ages, indicating that this blend maintains considerable strength even with partial clinker substitution. LC3-50 also shows enhanced strength compared to CEM, though it is slightly lower than that of LC3-60. In contrast, LC3-40 has reduced strength, likely because the increased clinker replacement diminishes both early and long-term strength. The dissolution of reactive silica and alumina from metakaolin in hydrated cement systems provides additional components that interact with portlandite (Shi et al., 2015). When the released silica is promoted, calcium silicate hydrate (C-S-H), the main binding phase in cement paste, is cre-

 ISSN: Online 2790-1637, Print 2790-1629
National Library of Libya, Legal number: 154/2018

ated. According to Richardson (2000), the modified form created here frequently has a lower Ca/Si ratio than regular C-S-H, which is linked to greater durability and less leaching susceptibility. When alumina is added to C-S-H, its nanostructure is further altered, producing a denser microstructure that enhances performance over the long run (Scrivener et al., 2015). Additionally, in the presence of carbonates, the alumina derived from kaolinite/metakaolin helps to generate AFm phases, particularly monocarboaluminate and hemicarboaluminate (Matschei et al., 2007). These carboaluminate compounds are stabilized by the combination of the aluminates and calcium carbonate, which is obtained from limestone filler (Lothenbach et al., 2008). In addition to consuming portlandite, which lowers the possibility of efflorescence and alkali leaching, this procedure improves the cement matrix's structural stability and refines the pore network (Hooton et al., 2007).

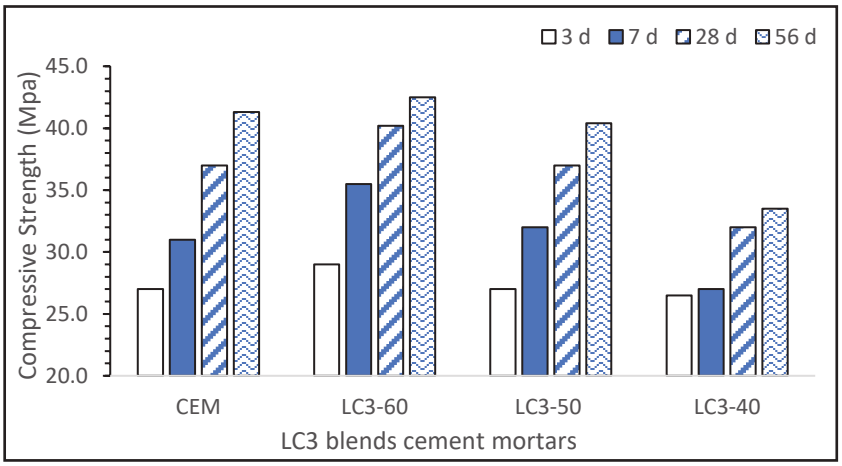

Figure 7. Compressive strengths of LC^3 blends cement mortars at different ages (days).

Strength Activity Index (SAI)

The Strength Activity Index (SAI) offers a reliable indirect measure of pozzolanic performance. As per ASTM C618, an SAI of ≥75% is required for a material to be considered pozzolani. To assess the effect of calcined clay - limestone blends (2:1 ratio) on reactivity, SAI was measured at 7 and 28 days for LC^3-based mixtures, as shown in Figure 8. It can be seen from the graph that all mixes exceeded the ASTM threshold. LC^3-60, LC^3-50 and LC^3-40 blends mortars show enhancement in early-age performance with SAI values of 113.3%, 103.2%, and 87.1%, respectively. LC^3-60 blend shows the highest SAI at both curing times, indicating it is the most effective in enhancing strength among the samples tested. While, LC^3-50 has a moderate SAI, suggesting it provides a good balance of strength but is less effective than LC^3-60. However, LC^3-40 blend has the lowest SAI, indicating it may not be as effective in improving strength compared to the others.

 ISSN: Online 2790-1637, Print 2790-1629
National Library of Libya, Legal number: 154/2018

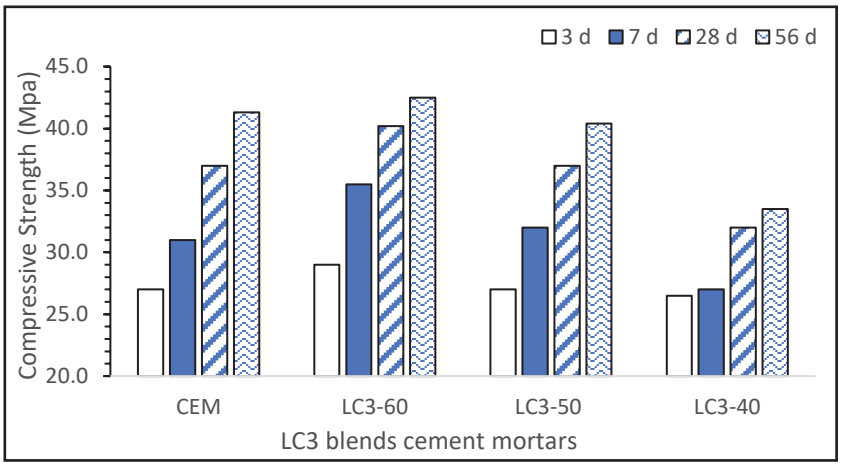

Figure 8. SAI for LC³ blends cement mortars at 7 and 28 days.

3.4.Flexural Strength:

Flexural strength results for CEM I and LC³ blends cement mortars with varying clinker replacement levels at 28 days are given in Figure 9. The Figure shows that LC³-60 blend exhibits the highest flexural strength (about 7.8 MPa), significantly outperforming the conventional CEM blend (about 5.9 MPa). LC³-50 also shows improved strength (about 7 MPa) over CEM, though slightly lower than LC³-60, indicating a potential trade-off between material proportions and performance. However, LC³-40 blend has the lowest strength of about 5.2 Mpa among the LC³ blends, even slightly below CEM.

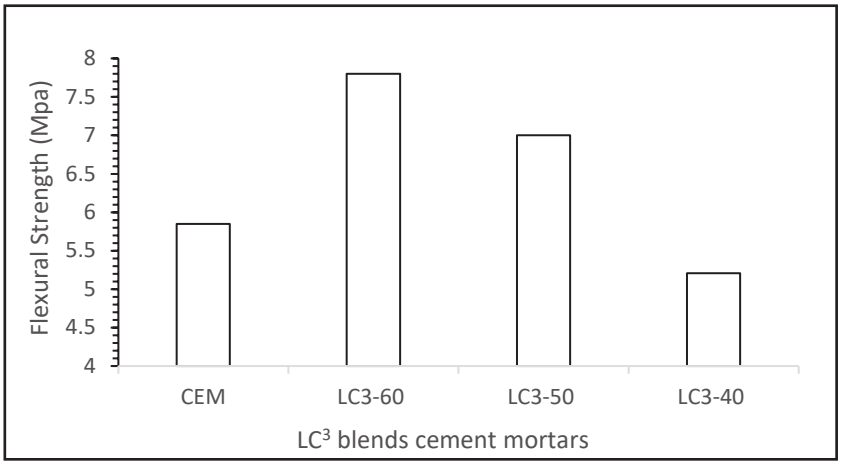

Figure 9. Flexural strengths of LC³ blends cement mortars at 28 days.

 ISSN: Online 2790-1637, Print 2790-1629
National Library of Libya, Legal number: 154/2018

3.5.Porosity:

As shown in Figure 10, LC^3 blends cement mortars (LC^3-60 and LC^3-50) exhibits significant reduction in porosity at all ages, with 28-day values of 9.6%, and 10.57%, respectively, lower than CEM I (11.7%). This improvement may be attributed to the high surface area of fine calcined clay particles, which enhances pozzolanic activity and promotes C-S-H formation, leading to a denser microstructure. These findings align with (Zunino & Scrivener, 2021) and (Zunino et al., 2022), who reported that the metakaolin-limestone synergy improves packing and promotes carboaluminate formation, reducing pore connectivity. However, LC^3-40 blend has the highest porosity across all curing periods, suggesting it has a lower density compared to the LC^3 blends, as Figure 5 illustrates.

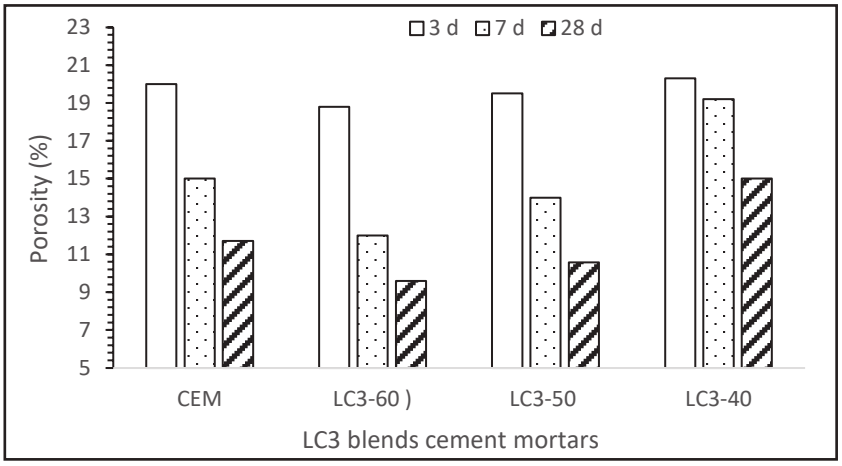

Figure 10. Porosity of LC^3 blends cement mortars at different ages.

3.6.Ultrasonic Pulse Velocity (UPV)

Figure 11 compares the ultrasonic pulse velocity (UPV) results of different cement mortar blends (CEM, LC^3-60, LC^3-50, and LC^3-40) over curing periods of 3, 7, and 28 days. As expected, UPV generally increases with curing time, indicating improved material properties as the cement hydrates and gains strength. CEM (presumably the control blend) serves as a baseline for comparing the performance of the LC^3 blends. The LC^3 blends (LC^3-60, LC^3-50, LC^3-40) show varying UPV values, which could suggest differences in their performance and hydration characteristics. Across all ages, LC^3-60 demonstrates the highest UPV values, peaking at 4.75 km/s at 28 days, signifying superior hardening and densification. While LC^3-50 shows increasing UPV, its values remain comparable to or slightly below CEM's at each stage, indicating moderate strength gain. In contrast, LC^3-40 consistently exhibits the lowest UPV, suggesting either reduced density or slower reaction kinetics relative to the other mixtures.

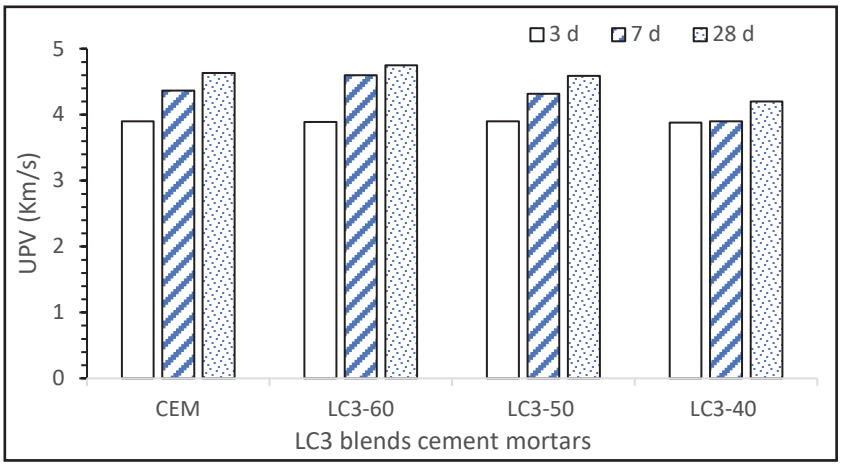

Figure 11. UPV of LC³ blends cement mortars at different ages.

5.CONCLUSIONS

Within this test program, LC³ mortars prepared with locally calcined kaolinite-rich clay and limestone achieved comparable 28-day compressive and flexural strengths to the OPC control at 50% clinker replacement, while exhibiting lower flow that will require admixture/water optimization. Mixtures at this replacement level also showed reduced accessible porosity, indicating microstructural densification. These findings suggest that 50% clinker replacement is a promising target for Southern-Libyan LC³ mortars. Further work should quantify durability (chloride ingress, carbonation, sulfate), report statistical confidence, and assess sustainability benefits with a simple CO_2/energy model.

6.ACKNOWLEDGMENT

Special appreciation is extended to Mrs. Fayza Najem and Mr. Hamad Al-Zalawi from the Benghazi Cement Factory for providing the required cement raw materials. Support from engineer Taha Al-Awjli (Libyan Technical Consultancy Company) during the study's experimental phase and Dr. Hanaa Al-Bakkoush (College of Public Health) for facilitating access to the furnaces used for clay calcination are also acknowledged. The authors would also like to thank Mr. Jamal Abdullah, Mr. Ahmed Bashir (Wadi Al-Shatti University), and Mr. Mohammed Adel (Post-Graduate Student) for assisting in providing the clay from the city of Sebha. Additionally, the authors would like to express their gratitude to civil engineering laboratory staff at the University of Benghazi for their support during the study's experimental stage.

REFERENCES

1.Akasha, A., M. "Using of Libyan Calcined Clay in Concrete". Calcined Clays for Sustainable Concrete:Springer, RILEM Bookseries, 2015, 555-561.

2.Antoni, M., Rossen, J., Martirena, F., & Scrivener, K. (2012). Cement substitution by a combination of metakaolin and limestone. Cement and Concrete Research, 42(12), 1579-1589. https://doi.org/10.1016/j.cemconres.2012.09.006

3.ASTM C 597-09. (2010). Standard Test Method for Pulse Velocity Through Concrete1. United States: American Society for Testing and Material., 04(02), 3-6.

4.ASTM C109/C109M-02. (2020). Standard Test Method for Compressive Strength of Hydraulic Cement Mortars. Annual Book of ASTM Standards, 04, 9.

5.ASTM C1437. (2007). ATSM C1437-07: Standard Test Method for Flow of Hydraulic Cement Mortar. Annual Book of ASTM Standards, 04, 6-7.

6.ASTM C305/C305-20. (2009). Standard Practice for Mechanical Mixing of Hydraulic Cement Pastes and Mortars of Plastic Consistency. ASTM International, 04, 3.

 ISSN: Online 2790-1637, Print 2790-1629
National Library of Libya, Legal number: 154/2018

7.ASTM C778. (2009). Standard Specification for Standard Sand. Annual Book of ASTM Standards, 04, 16.

8.ASTM International. (2021). ASTM C348-21: Standard test method for flexural strength of hydraulic-cement mortars. ASTM International. https://www.astm.org/c0348-21.html

9.Balasubramanian, N., & Sarangapani, C. (2024). A review on the factors influencing the performance of sustainable ternary cement composites. Environment, Development and Sustainability, 26(10), 24569-24596. https://doi.org/10.1007/s10668-023-03685-0

10.British Standards Institution. (2011). BS EN 197 1:2011 Cement - Part 1: Composition, specifications and conformity criteria for common cements. British Standards Institution (BSI), London, UK.

11.Chaipanich, A., Sansuthum, N., Chomyen, P., Wianglor, K., & Aodkeng, S. (2024). Phase formations , Compressive Strength and Microstructure of Environmentally Friendly Thai Lopburi Calcined Clay - Limestone Cement Mixes. Chiang Mai Journal of Science, 51(6) :e2024089. https://doi.org/10.12982/CMJS.2024.089

12.Dhandapani, Y., Santhanam, M., Kaladharan, G., & Ramanathan, S. (2021). Towards ternary binders involving limestone additions -A review. Cement and Concrete Research, 143, 106396. https://doi.org/10.1016/j.cemconres.2021.106396

13.Ferrari, L., Bortolotti, V., Mikanovic, N., Ben-Haha, M., & Franzoni, E. (2023). Influence of Calcined Clay on Workability of Mortars with Low-carbon Cement. NanoWorld Journal, 9 (Special Issue 2), S30-S34. https://doi.org/10.17756/nwj.2023-s2-006

14.Hawkins, P., Tennis, P., & Detwiler, R. (2003). The use of limestone in Portland cement: A state-of-the-art review (Portland Cement Association, PCA R&D Serial No. 2117, 1-44). Skokie, IL: Portland Cement Association.

15.Hooton, R. D., Nokken, M. R., & Thomas, M. D. A. (2007). Portland-limestone cement: State-of-the-art report. Journal of Materials in Civil Engineering, 19(9), 837-854.

16.Kafodya, I., Basuroy, D., Marangu, J. M., Kululanga, G., Maddalena, R., & Novelli, V. I. (2023). Mechanical Performance and Physico-Chemical Properties of Limestone Calcined Clay Cement (LC3) in Malawi. Buildings, 13(3), 740. https://doi.org/10.3390/buildings13030740

17.Lin, R. S., Lee, H. S., Han, Y., & Wang, X. Y. (2021). Experimental studies on hydration–strength–durability of limestone-cement-calcined Hwangtoh clay ternary composite. Construction and Building Materials, 269, 121290. https://doi.org/10.1016/j.conbuildmat.2020.121290

18.Lothenbach, B., Matschei, T., Möschner, G., & Glasser, F. P. (2008). Thermodynamic modelling of the effect of temperature on the hydration and porosity of Portland cement. Cement and Concrete Research, 38(1), 1-18.

19.Matschei, T., Lothenbach, B., & Glasser, F. P. (2007). The AFm phase in Portland cement. Cement and Concrete Research, 37(2), 118-130.

20.Nararueang, A., Rianyoi, R., Aodkeng, S., & Chaipanich, A. (2024). Compressive Strength, Flowability, and Ultrasonic Pulse Velocity Tests of Portland Cement-Fly Ash-Calcined Clay Mortars. Suranaree Journal of Science and Technology, 31(2), 1-7. https://doi.org/10.55766/sujst-2024-02-e03738

21.Richardson, I. G. (2000). The nature of the hydration products in hardened cement pastes. Cement and Concrete Composites, 22(2), 97-113.

22.RILEM Technical Committee CPC 11.3. (1994). Absorption of water by concrete by immersion under vacuum (RILEM Technical Recommendation CPC 11.3). In RILEM Recommendations for the Testing and Use of Construction Materials . E & FN Spon.

23.Sabir, B., Wild, S., & Bai, J. (2001). Metakaolin and calcined clays as pozzolans for concrete: A review. Cement and Concrete Composites, 23(6), 441-454. https://doi.org/10.1016/S0958-9465(00)00092-5

24.Scrivener, K. L., Martirena, F., Bishnoi, S., & Maity, S. (2015). Calcined clay limestone cements (LC^3). Cement and Concrete Research, 114, 49-56.

25.Shao, J., Guo, S., & Wang, H. (2025). A review of the performance, sustainable applications, and research challenges of limestone-calcined clay-cement (LC3) systems. Coatings, 15(5), 611. https://doi.org/10.3390/coatings15050611

26.Shi, C., Jiménez, A. F., & Palomo, A. (2015). New cements for the 21st century: The pursuit of an alternative to Portland cement. Cement and Concrete Research, 41(7), 750-763.

27.Snellings, R. (2016). Assessing, understanding and unlocking supplementary cementitious materials. RILEM Technical Letters, 1, 50-55. https://doi.org/10.21809/rilemtechlett.2016.12

28.Takhi, K., Bouhamou, N. E., Bouziani, T., & Kiboub, M. Y. (2024). A study on fresh, mechanical, and thermal properties of limestone calcined clay cement (LC3) blended with cementitious materials. STUDIES IN ENGINEERING AND EXACT SCIENCES, 5(2), e8034. https://doi.org/10.54021/seesv5n2-228

29.Taylor, H. F. W. (1997). Cement chemistry (2nd ed.). Thomas Telford Publishing.

30.Yu, J., Wu, H. L., Mishra, D. K., Li, G., & Leung, C. K. (2021). Compressive strength and environmental impact of sustainable blended cement with high-dosage Limestone and Calcined Clay (LC2). Journal of Cleaner Production, 278, 1-14 (Article 123616). https://doi.org/10.1016/j.jclepro.2020.123616

31.Zunino, F., & Scrivener, K. (2021). The reaction between metakaolin and limestone and its effect in porosity refinement and mechanical properties. Cement and Concrete Research, 140, 106307. https://doi.org/10.1016/j.cemconres.2020.106307

32.Zunino, F., Dhandapani, Y., Ben Haha, M., Skibsted, J., Joseph, S., Krishnan, S., Parashar, A., Juenger, M. C. G., Hanein, T., Bernal, S. A., Scrivener, K. L., & Avet, F. (2022). Hydration and mixture design of calcined clay blended cements: review by the RILEM TC 282-CCL. Materials and Structures/Materiaux et Constructions, 55, 1-33 (Article 234). https://doi.org/10.1617/s11527-022-02060-1

 ISSN: Online 2790-1637, Print 2790-1629
National Library of Libya, Legal number: 154/2018

Scientific Journal of University of Benghazi

SJUOB (2025) 38 (2) Applied Sciences: Ibrahim. et . al, 56 – 65
www.sjuob.uob.edu.ly

Comparison Between Green And Chemical Synthesis Of Copper Nanoparticles: Characterization And Antibacterial Activity

Dalal M. Ibrahim[1]*, Rania S. Bendaba[2], Rehab a yaakub Hesien[1]

1.Department of Chemistry, Omar Al-Mukhtar University, Al Baida, Libya.
2.Department of Chemistry, Libyan Academy, Tubruk.

DOI: 10.37376/sjuob.v38i2 | Received:30/08/2025 | Accepted:28/11/2025 | Publishing: 23/12/2025

ABSTRACT

Nanoparticles are often associated with their small size and numerous applications. The synthesis process is equally important since it determines the size and properties of the nanoparticles. Additionally, green synthesis provides an economical, ecologically beneficial, and sustainable substitute. Researchers have focused on copper nanoparticles (NPs) due to their unique characteristics, which include optical, antibacterial, and electrical capabilities that depend on size and form. Two techniques are becoming more well-known in this field for producing silver nanoparticles. The green method and chemical reduction were used to create copper nanoparticles, and the two samples' optical, antimicrobial, and structural properties were examined. An extract derived from lemon fruit was incorporated into the environmentally friendly procedure. Furthermore, trisodium citrate was used as a reducing agent in the chemical procedure, and several techniques were used to characterize the nanoparticles. These techniques include X-ray diffraction (XRD), ultraviolet-visible spectroscopy (UV-Vis), scanning electron microscopy (SEM), and antibacterial activity. The XRD analysis revealed that the particles were crystalline in form and that the green-produce variation's crystal sizes (4.6 nm) were greater than those of the chemical reduction variant (2 nm). The shape of the chemically produced nanoparticles is unclear, whereas the green approach coats the generated nanoparticles with the biological materials in lemon extract. The antibacterial evaluation was completed using the agar well diffusion method. The particles' SEM images showed that they were aggregating into polyhedral and leaf-shaped particles. In the aqueous solution containing copper nanoparticles, the chemically generated absorption peak was located at 300 nm in the UV-visible spectrum, whereas the green synthesized absorption peak was located at 260 nm. This included Escherichia coli O157:H7 and Staphylococcus aureus as the bacteria in the medium. The green had a larger zone of bacterial growth inhibition. synthesized variant in different concentrations of 20 mg, 40 mg, and 60 mg, which were 22 mm, 25 mm, and 28 mm in Escherichia coli and 14 mm, 24 mm, and 26 mm in Staphylococcus aureus, respectively. Conclusions: The improved antibacterial responses of the green-produced versions were caused by the accelerated rate at which the organic chemicals in the lemon fruit extract stabilized the nanoparticles.

KEYWORDS: Nanoparticles, green synthesis, chemical synthesis, antibacterial

Corresponding Author: Dalal M Ibrahim, *dalal.m.ibrahim@omu.edu.ly*

 ISSN: Online 2790-1637, Print 2790-1629
National Library of Libya, Legal number: 154/2018

1.INTRODUCTION

Nanoparticles are particles that are between one and one hundred manometers in size. For any object that is 'one billionth,' or 10^{-9}, of another, the prefix 'nano' is used. Ordinary materials often exhibit unusual and distinctive characteristics when reduced to the nanoscale, such as electrical conductivity, chemical reactivity, super paramagnetic behavior, exceptional strength, and other characteristics that the same material lacks at the macro- or microscale. Technology is being developed to limit any dangers to environmental factors and human health related to manufacturing (1-4). The application of nanotechnology products, as well as promoting the substitution of new, environmentally friendly nano-products for current ones. This is known as "green nanotechnology (5,6).

The branch of science and engineering that focuses on materials is called nanotechnology, according to (7). According to (8), nanoscience is the study of phenomena at particle sizes between 1 and 100 nm, and nanomaterials are materials with ordered components at least one dimension smaller than 100 nm. Nanoparticle-derived nanomaterials: In the past decade, nanoparticles have emerged as a unique class of materials. Because of their superior conductivity, metal nanoparticles have garnered more scientific interest than metal oxide nanoparticles (9). Metal nanoparticles are discrete particles with sizes ranging from one to one hundred nm; they are not part of a chemical bond between metals. In contrast to their equivalent in bulk metal, metal nanoparticles (NPs) differ greatly from their counterparts in bulk metal in that. In addition to being large and having a higher surface-to-volume ratio, these objects also have lower energy state densities (10, 11). As a result, they exhibit more specificity and chemical activity than bulk metals, making them desirable for use as catalysts (12, 13).

The mechanical, optical, magnetic, electrical, and chemical characteristics of metal nanoparticles differ greatly from bulk metals because of their size effects, often referred to as quantum effects, and high surface-to-volume ratio (14, 15). Nanoparticles have drawn significant interest from researchers because of their special qualities and wide variety of uses.

The "bottom-up" and "top-down" approaches are the two methods used to create nanoparticles (16, 17). A top-down approach uses size reduction from a suitable starting material for nanoparticle manufacturing (18). Size reductions are achieved using a variety of physical and chemical techniques. Imperfections created in a top-down manner in the nanoparticles' surface structure pose a substantial constraint because the chemistry of the surface and additional physical characteristics of the nanoparticles largely rely on the surface structure (19, 20). Bottom-up synthesis combines smaller entities to produce nanoparticles (21,22).

As per (18), this technique entails the initial creation of smaller entities that are subsequently put together to create final particles with sizes in the nanoscale range. The bottom-up approach is implemented through the use of chemical and biological methods. Although biological processes need very little energy and are conducted in ecologically benign settings, the production of nanoparticles via chemical and physical methods requires a lot of energy, which is harmful to the environment, and involves dangerous substances (23-25).

Although the synthesis of metal nanoparticles by biological methods takes longer than chemical methods, this time has been decreased by employing the appropriate bacteria or organisms (26). Thus, the low cost, environmental friendliness, and one-step, large-scale process are the benefits of biological approaches over chemical and physical procedures. It is possible to produce nanoparticles without using dangerous chemicals, high pressures, temperatures, or energy (27, 28). It is well known that bacteria can produce nanoparticles through biological processes (29). The

 ISSN: Online 2790-1637, Print 2790-1629
National Library of Libya, Legal number: 154/2018

cost of controlling and growing microorganisms is higher than that of plant extracts, although using microbes to synthesize nanoparticles is easily scalable, environmentally benign, and appropriate for use in medical applications. Due to its low cost, plant-mediated synthesis of metal nanoparticles can be a valuable and economical alternative to large-scale manufacturing (30, 31). Therefore, this study aims to develop an environmentally friendly, cost-effective, and simple synthesis method for metal nanoparticles, also the application of synthesized nanoparticles as antibacterial effect on Gram-negative bacteria (Escherichia coli) and Gram-positive bacteria (Staphylococcus aureus).

2.EXPERIMENTAL

2.1.Green Method

To create the lemon fruit extract, the lemon fruit was cut and transferred to a 250-mL beaker with 200 mL of deionized water. The mixture was heated at 80 °C for 10 minutes and subsequently filtered through 125-mm filter paper. Copper sulphate pentahydrate (Cu_2SO_4) is used to prepare green Nanoparticles of copper for the synthesis of nanoscale nanoparticles of copper from lemon fruit extract; H_2O was utilized as a precursor. Eight grams of copper sulphate pentahydrate were added to 200 milliliters of lemon fruit extract, and this mixture was stirred magnetically for two hours, forming a dark green paste. The mixture was then calcined to produce a black powder of copper nanoparticles.

2.2.Chemical Method

Initially, a 100 mL aqueous solution of copper sulphate pentahydrate ($Cu_2SO_4.5H_2O$) at 0.01M was prepared. Next, 100 mL of tri-sodium citrate ($Na_3C_6H_5O_7.2H_2O$) at 0.1M was incorporated into the solution above and was stirred at 80°C for an hour. Green powder formed and was dried for half an hour at 200°C. Lastly, 100 mL of potassium hydroxide (KOH) 1M was progressively added to the mixture until the pH reached 12. After that, it was stirred for 30 minutes.

2.3.Antimicrobial Action:

Cultures of bacteria: The nutrients agar medium plate cultures were employed to cultivate the bacteria. 250 milliliters of sterile distilled water were used to dissolve 7 grams of powder to create the medium. Following a 15-minute autoclaving at 121 °C to sanitize the medium, the bacteria were grown and incubated for 24 hours at 37 °C. Antimicrobial test: Green synthesis and the antibacterial properties of chemical synthesis. By applying the agar disk diffusion technique, copper nanoparticles will be examined on two species of bacteria, Escherichia coli and Staphylococcus aureus, that were cultured for 72 hours in stable cultural media.

3.RESULTS AND DISCUSSION

3.1.Physical Properties

The physical properties of Green and Chemical Synthesized Copper nanoparticles are shown in Table 1

 ISSN: Online 2790-1637, Print 2790-1629
National Library of Libya, Legal number: 154/2018

Table 1. Physical properties of green and chemical copper nanoparticles

Nanoparticle	Melting point	Solubility in water	Solubility in alcohol	Solubility in DMSO	Solubility in DMF	Color and texture
Green Cu nanoparticles	Over 350°C	Slow solubility	Non soluble	Slow solubility heating	Slow solubility with heating	Black hard powder
Chemical Cu nanoparticles	Over 350°C	Soluble	Non soluble	Slow solubility with heating	Slow solubility with heating	Pale Green soft powder

3.2.Ultra Violet-Visible Spectroscopy

Each sample was diluted with 0.005 mg in 5 dimethyl form amides, sonicated for 20 minutes, and then scanned in the 200–400 nm wavelength range using a BMG LABTECH spectrophotometer (Ortenberg, Germany).

As seen in Figure 1 below, the absorption band in the UV-VIS spectroscopy of Chemical Copper nanoparticles and Green Copper nanoparticles was located at 300 nm, with absorption values of 1.5324 and 1.651, respectively. Copper nanoparticles formed in accordance with studies that suggested that copper nanoparticles created between 200 and 350nm, as figure 1 shows the absorption band at 300nm verified the formation of copper nanoparticles; The absorbance intensity dropped as the wavelength grew, suggesting that formation did not take place at a very long wavelength.

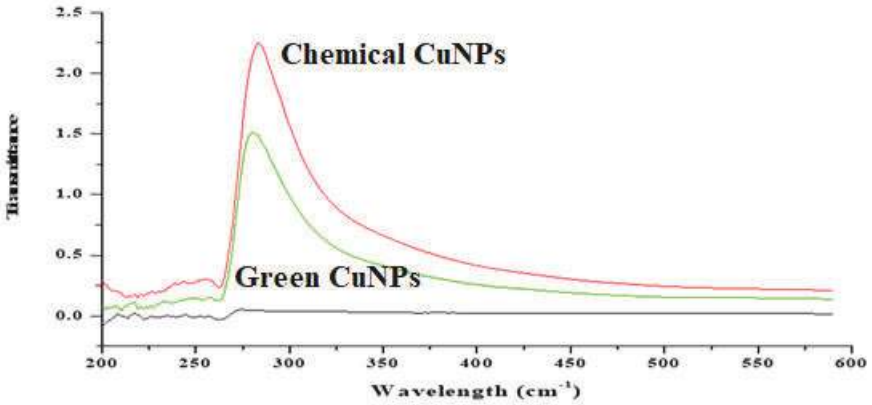

Figure1. UV-VIS spectrum analysis

3.3.Scanning Electron Microscopy

SEM was used to investigate the shape of artificially created copper nanoparticles. The SEM images of chemically synthesized copper nanoparticles and green synthesized copper nanoparticles are shown in Figure 2. The experimental results showed that the SEM images of the chemically synthesized nanoparticles showed aggregation of the particles with polyhedral and leaf-shaped particles. In contrast, the green method produced nanoparticles whose shape is obscured in SEM images because they are coated in biological molecules in the lemon fruit extract. However, it is evident from the images that green nanoparticles are smaller than chemically produced ones, which indicates a large ratio of surface area to volume. These results are consistent.

 ISSN: Online 2790-1637, Print 2790-1629
National Library of Libya, Legal number: 154/2018

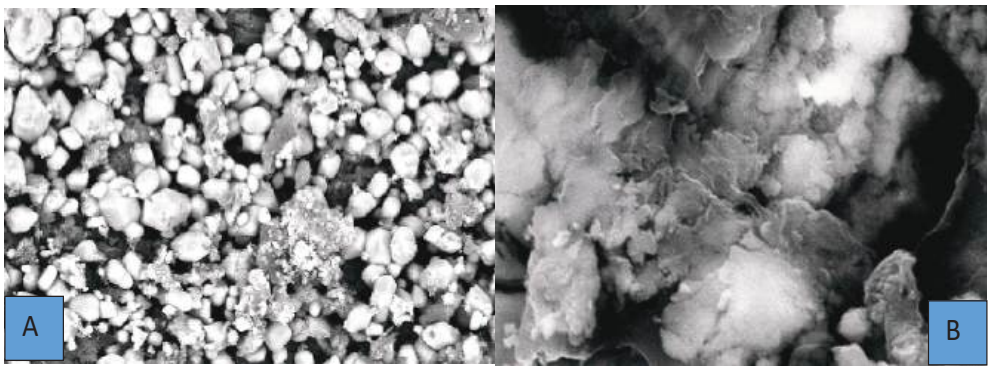

Figure 2. SEM Images of (A) chemical Copper nanoparticles and(B) Green Copper nanoparticles

3.4.X-Ray Diffraction Analysis

The copper nanoparticles' X-ray diffraction patterns produced by lemon fruit extract are shown in Figures 3 and 4. The copper nanoparticles synthesized in green exhibit a more acute diffraction peak value, indicating a higher percentage of crystalline phases. On the other hand, the size of the crystallite was established using the Debye Scherer equation:

$D=K\lambda / (\beta \cos \theta)$

Here, K is the dimensionless form factor (~0.94), μ is the radiation wave length, and θ is the Bragg angle. β is also the complete width at half maximum of the corresponding peak. D is primarily the ordered domains' primary size, which is regarded as being equivalent to the size of the particle (applicable for only particles less than 100 nm). From the values in the diffraction pattern of The Green copper nanoparticles, the particle size can be calculated as below.

$D=K\lambda/(\beta \cos \theta)$

$D=(0.94\times1.54)/(4.73 \cos 9)$

$D=4.6$ nm

For less 2θ value, and for a higher one, it becomes as below.

$D=K\lambda/(\beta \cos \theta)$

$D=(0.94\times1.54)/(1.13 \cos 42.5)$

$D= 1.7$nm

So, from XRD, the particle size of the Green Copper Nanoparticle is from 1.7 to 4.6 nm, and from the X-ray diffraction pattern values of the chemical copper nanoparticles, the particle size of chemically synthesized copper nanoparticles is calculated as

$D=K\lambda/(\beta \cos \theta)$

$D=(0.94\times1.54)/(1.0 \cos 49)$

$D=0.3$nm

And for the less value of 2θ, the smaller particles the particle size:

$D=K\lambda/(\beta \cos \theta)$

$D=14.56/8.36$

$D=1.74 \sim 2$nm

From the results of XRD and by applying the Debye Scherer equation, the particle size of Green Copper nanoparticles is between 3nm-16nm, smaller than the chemically synthesized 0.3-2nm in size.

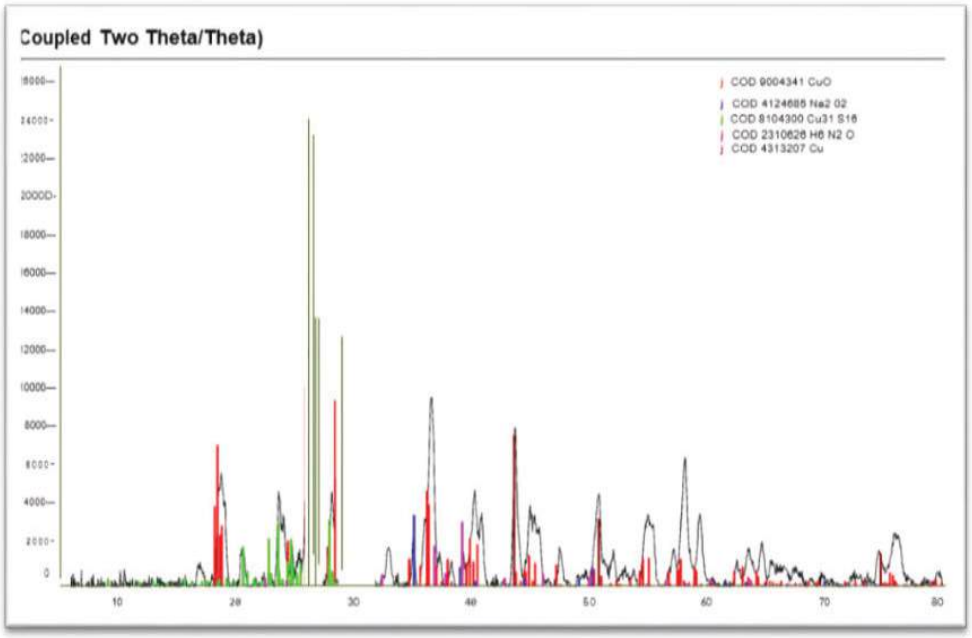

Figure3. XRD diffraction pattern of Green Synthesized Copper nanoparticles

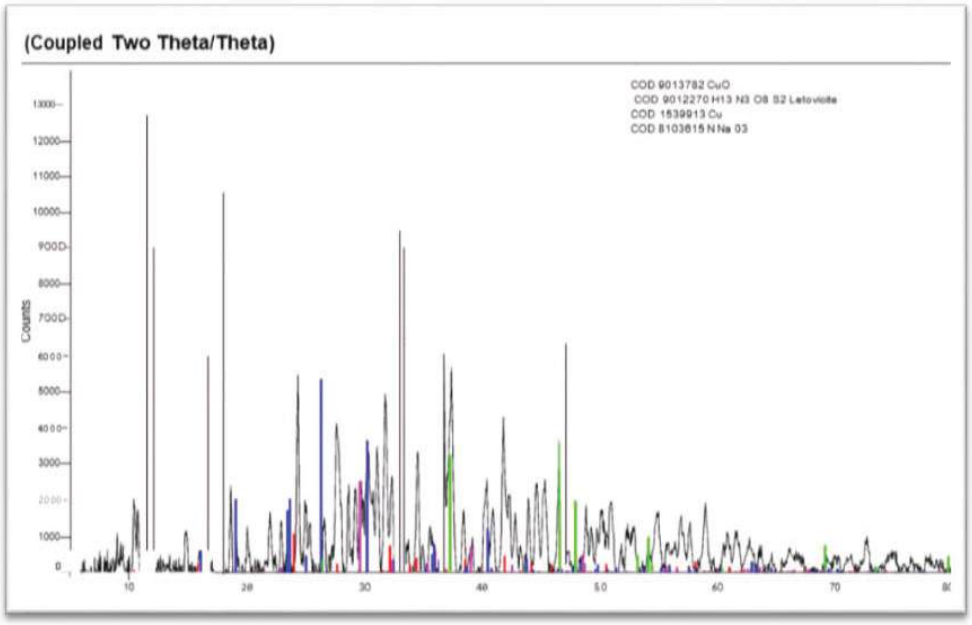

Figure 4. XRD diffraction pattern of chemically synthesized Copper nanoparticles

 ISSN: Online 2790-1637, Print 2790-1629
National Library of Libya, Legal number: 154/2018

3.5.Antibacterial activity

Two different species of bacteria were used to test the antibacterial activity. Gram-negative bacteria, Gram-positive Staphylococcus aureus, and Escherichia coli are all represented in the antibacterial action of chemical and green copper nanoparticles. Using the Agar diffusion method, the products were used in powder form at concentrations of 20, 40, and 60 mg. All the concentrations were applied to the surface of the culture plates, and the plates were then incubated upside down at 37°C for a whole day(35). After the inhibitory effects of the substances were identified, it was found that the zones of suppression of bacterial growth produced by green and chemical copper nanoparticles differed from one another. Nanoparticles' antibacterial efficacy is a size-dependent property that improves with a reduction in particle size; for E. coli (Gram-negative), green CuNPs produced inhibition zones of 22–28 mm, whereas chemically synthesized CuNPs produced 12–23 mm. A similar trend was observed for S. aureus (Gram-positive), with green CuNPs producing 14–26 mm inhibition zones compared to 10–28 mm for chemical CuNPs. The enhanced activity of green nanoparticles may be attributed to the presence of bioactive phytochemicals from the lemon extract, such as flavonoids, polyphenols, and citric acid, which can act synergistically with the copper ions to disrupt bacterial membranes more effectively (32,36) Such natural capping agents can improve nanoparticle stability, dispersion, and surface reactivity, all of which increase antibacterial efficiency (33,34). However, Green Copper nanoparticles increase the zone of inhibition more than Chemical Copper nanoparticles, and the measurements of the inhibition zone are tabulated in Tables 3 and 4. Green Copper nanoparticles exhibit more antibacterial potential than Chemical Copper nanoparticles because they have smaller particle sizes and higher surface areas. The tables (2–3) and figures (5–6) provided illustrations of the results.

Table 2 Antibacterial measurements of green copper nanoparticles

Sample	Bacteria	Weight of the sample (mg)	Bacteria type	Zone of inhibition D(mm)
Green Copper Nano-particles	Escherichia coli	20	Gram negative	22
		40		25
		60		28
	Staphylococcus aureus	20	Gram positive	14
		40		24
		60		26

Table 3 Antibacterial measurements of Chemical Copper Nanoparticles

Sample	Bacteria	Weight of the sample (mg)	Bacteria type	Zone of inhibition D(mm)
Chemical Copper Nano-particles	Escherichia coli	20	Gram negative	12
		40		15
		60		23
	Staphylococcus aureus	20	Gram positive	10
		40		20
		60		28

 ISSN: Online 2790-1637, Print 2790-1629
National Library of Libya, Legal number: 154/2018

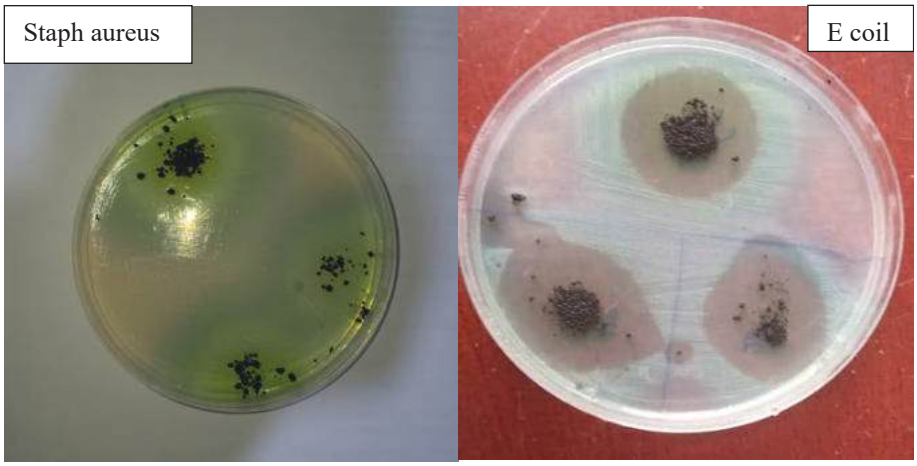

Figure 5. Antibacterial effect of green copper nanoparticles at three concentrations on E. coli and staph aureus.

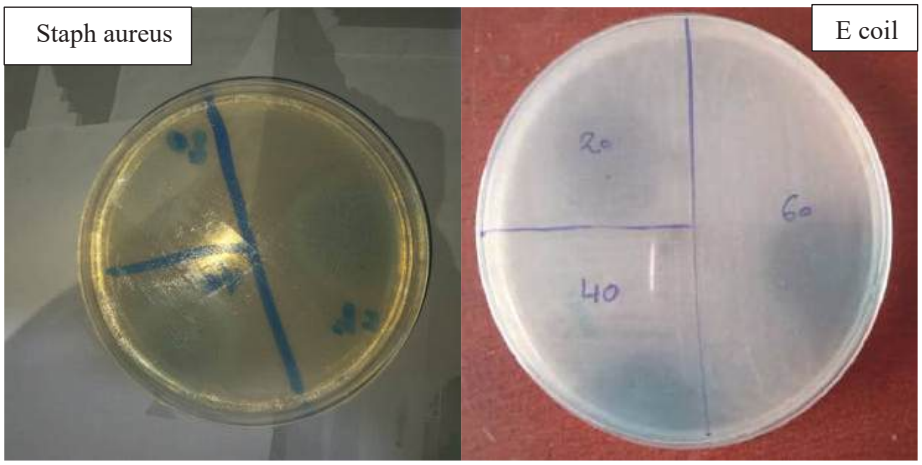

Figure 6. Antibacterial effect of chemical copper nanoparticles at three concentrations on E. coli and Staph aureus.

4.CONCLUSION

In summary, two different methods were employed to produce copper nanoparticles: the green method, which utilized the aqueous extract from lemon fruit, and the chemical reduction method, which used trisodium citrate. The aqueous extract from lemon fruit is free of the dangerous chemicals used in the chemical process. The phytochemicals in the lemon fruit extract, however, not only aid in lowering the particle sizes but also in adequately stabilizing them. Furthermore, the optical band gaps of the two processes were about the same, and the green approach's average copper nanoparticle size was greater than the chemical method's (2 nm). Additionally, using the green technique increased the lemon fruit extract antimicrobial effectiveness. Consequently, a comparison of the features of the two variations leads to the conclusion that green synthesis is more effective than chemical reduction in producing copper nanoparticles.

5.ACKNOWLEDGMENT

The authors are grateful to Omar Al-Mukhtar University, especially the Department of Chemistry.

 ISSN: Online 2790-1637, Print 2790-1629
National Library of Libya, Legal number: 154/2018

REFRENCES

1.Ahmadi.S, & Izanloo.C. (2023). Biosynthesis of iron oxide nanoparticles at different temperatures and its application for the removal of zinc by plant-mediated nanoparticle as an eco-friendly nanoadsorbent. results in chemistry.

2.Abusaad.S. (2018). Nanotechnology: concepts, importance and the current state of scientific research. the first conference for engineering sciences and technology.

3.Abbas. I.K., & Adam. K.A. (2023). Synthesis and characterization of magnesiumoxide nanoparticles by atmospheric non-thermal plasma jet. Kuwait journal of science.

4.Alkac.I, Cereci.B, Timuralp.C, & Sen.F. (2021). nanomaterials for direct alcohol fuel cells: characterization, design, and electrocatalysis micro and nanotechnology.

5.Al-zaqri. N, Mohana.V, Boshaala.A, Umamakeshvari.K, & Muthuvel.A. (2022). Green synthesis of nickel oxide nanoparticles and its photocatalytic degradation and antibacterial activity. journal of materials science: materials in electronics.

6.Amaliyah, S., Purti Pangesta, D., Masruri, M., Sabarudin, A., & Bambang Sumitro, S. (2020). Green synthesis and characterization of copper nanoparticles using Piper retrofractum Vahl extract as bioreductor and capping agent. Heliyon.

7.Salata, O. V. (2004). Applications of nanoparticles in biology and medicine. Journal of nanobiotechnology, 2(1), 1-6.

8.Luque, R., & Varma, R. (2013). Sustainable preparation of metal nanoparticles: Methodes and applications. Cambridge(UK): Royal Society of Chemistry.

9.Ibrahim, D., Abdelghani, K., Anwagy, S., & Rizkallah, R. (2024). Synthesize Iron Oxide and Zinc Oxide Nanoparticles Using Plant Extracts. AlQalam Journal of Medical and Applied Sciences, 11-14.

10.Ozin, G., Arsenault, A., & Cademartiri, L. (2000). Nanochemistry: A chemical Approach to Nanomaterials. Cambridge, UK.

11.Chen, M., Cai, Y., Yan, Z., Goodman, D., & and Am, J. (n.d.). Chem.Soc. doi:128(2006)63415.

12.Bruss, A., Gelesky, M., Machado, G., & Dupont, J. (2006). Journal of Molecular Catalysis. doi:252(2006) 212.

13.Firooz, A., Mahjoub, A., & Khodadadi, A. (2011). World Academy of science, Engineering and technology. doi:76(2011) 138.

14.El-Sayed, M. (2001). Accounts of chemical research. doi:34(2001) 257

15.Alivisator, A. (1996). Journal of Physical Chemistry. doi:100 (1996) 13226

16.Speur, S. (2008). Nanotechnology: Technical Basics and Applications. Hannover: Vincentz.

17.Anada Murthy, H., Desalegn, T., Kassa, M., Abebe, B., & and Assefa, T. (2020). Synthesis of Green copper nanoparticles using medicinal plant Hagenia abyssinica (Brac) JF.Gmel. Leaf Extract: antimicrobial properties. (V. P. Tolstoy, Ed.) Hindawi Journal of Nanomaterials.

18.Meyers, M., Mishra, A., & Benson, D. (2006). prog. Mater Sci. doi:51(2006) 427

19.Thakkar, K., Mhatre, S., & Parikh, R. (2010). Nanomad. Nanotechnol. Biol. Med. doi:6(2010) 257

20.Ansilin, S., Kavya Nair, J., Aswathy, C., Rama, V., Peter, J., & Jeyachynthaya, J. (2016). Green synthesis and characterization of Copper oxide nanoparticles using Azadirachta indica (Neem) Leaf Aqueous Extract. Journal of nanoscience and technology. Retrieved from www.jacsdirectory.com/jnst

21.Mukhrjee, P., Ahmad, A., Mandal, D., Senapati, S., Sainkar, R., & Khan, M. (2001). Nano Lett. doi:1 (2001) 515

22.Badhe.N, Shitole.P, Chaudhari.Y, Matkar.S, Jamdhade.P, & Gharat.T. (2023). Nanoparticles in cosmetics: the safety and hidden risks. international journal of biological engineering.

23.Baig.N, Kammakakam.I, & Falath.W. (2021). Nanomaterials: a review of synthesis methods, prop-

erties, recent progress, and challenges. RPYAL SOCIETY OF CHEMISTRY. doi:10.1039/D0MA00807A

24.Bajpai.V, Kamle.M, Shukla.S, Mahato.D.K, Chandra.P, Hwang.S.K, . . . Kyu-han.Y. (2018). Prospects of using nanotechnology for food preservation, safety, and security. journal of food and drug analysis, pp. 1201-1214. Retrieved from https://doi.org/10.1016/jfda.2018.06.011

25.Barhoum, A. (2016). History and development of nanostructures and materials. research Gate. Retrieved from https://www.researchgate.net/publication/309733691

26.Gorbani, H., Safekordi, A., Attar, H., & Sorkhabadi, S. M. (25, 2011). Chem. Biochem. Eng. Q. doi:25 (2011) 317

27.Sastry, M., Ahmad, A., Khan, M., & Kumar, R. (2003). Curr SCi. doi:85(2003) 162

28.Batool, M. Q. (2018). Biosynthesis of copper nanoparticales by using Aloe barbadensis leaf extract. Interventions in pediatric dentistry open accesss journal.

29.Sanghi, R., & Verma, P. (2010). Green Chem. Environ. Sustainable. doi:15(2010) 315

30.Bayda.S, Adeel.M, Tiziano.T, Cordani.M, & Rizzolio.F, &. (2019). The history of nanoscince and nanotechnology: from chemical-physical applications to nanomedicine. molecules.

31.Bayda.S, Adeel.M, Tuccinardi.T, Cordani.M, & Rizzolio.F, &. (2019). The history of nanoscience and nanotechnology: from chemical -physical applications to nanomedicine. Exploitation of multifunctional nanomaterials for biological applications.

32.Rai, M., Yadav, A., & Gade, A. (2012). Current trends in phytosynthesis of metal nanoparticles and their applications. Biotechnology Advances, 31(2), 346–356.

33.Ravani, S. (2011). Green synthesis of metal nanoparticles using plants. Green Chemistry, 13(10), 2638–2650.

34.Ahmed, S., Saifullah, Ahmad, M., Swami, B. L., & Ikram, S. (2016). Green synthesis of metal nanoparticles using plants and their biological applications. Journal of Advanced Research, 7(1), 17–28.

35.Lithi, I. J., Nakib, K. I. A., Chowdhury, A. M. S., & Hossain, M. S. (2025). A review on the green synthesis of metal (Ag, Cu, and Au) and metal oxide (ZnO, MgO, Co_3O_4, TiO_2) nanoparticles using plant extracts for developing antimicrobial properties. Nanoscale Advances, 7, 2446–2473.

36.Abbasi, S., Abbasi, H. A., Atif, M., Anjum, M. N., & Rahman, U. U. (2024). Green Synthesis of Copper Nanoparticles from Artemisia maritima: Characterization and Evaluation of Antibacterial Properties. Futuristic Biotechnology, 4(04), 56–62.

Scientific Journal of University of Benghazi

SJUOB (2025) 38 (2) Applied Sciences: Alkafrawi. et . al, 66 – 72
www.sjuob.uob.edu.ly

Zero-Shot Slice Policy Transfer for Cloud-RAN Resource Allocation under Fronthaul and SLA Constraints.

Ismail M. Alkafrawi[1]*, Ibrahim M. M. Mohamede[2], Abdulla Ali Abouda[3]

1.Electrical Engineering Department, Faculty of Engineering, University of Benghazi, Benghazi, Libya.
2. Electrical Engineering Department, Faculty of Engineering, University of Omar Al-Mukhtar , Al Bayda, Libya.
3. Almadar Aljadid Company.

DOI: 10.37376/sjuob.v38i2 | Received:29/08/2025 | Accepted:08/12/2025 | Publishing: 23/12/2025

ABSTRACT

Cloud RAN requires fast, SLA aware resource allocation across heterogeneous slices (eMBB, URLLC, mMTC). Training a dedicated controller for every slice is impractical; policies must generalize to unseen slice semantics spanning latency, reliability, rate, burstiness, and mobility. A coupled radio–compute–fronthaul allocation problem is formulated, and Zero Shot Slice Policy Transfer (ZSPT) is introduced as a semantics to policy mapping that operates without per slice training by distilling a high quality convex surrogate into a lightweight scheduler. In this paper zero shot performance was evaluated against Proportional Fair (PF) and the convex surrogate, reporting throughput, Jain's fairness, UE rate percentiles, and SLA violation probability with bootstrap 95% confidence intervals. In a representative scenario, ZSPT matched PF on unseen slices, while the convex surrogate increased fairness and substantially raises 5th percentile UE rates.

KEYWORDS: RAN slicing, Cloud RAN, zero shot learning, convex optimization, proportional fair, fronthaul, SLA.

Corresponding Author: Ismail M. Alkafrawi.

 ISSN: Online 2790-1637, Print 2790-1629
National Library of Libya, Legal number: 154/2018

1.INTRODUCTION

Network slicing exposes a single radio access network (RAN) to heterogeneous service–level agreements (SLAs) spanning enhanced mobile broadband (eMBB), ultrareliable lowlatency communications (URLLC), and massive machinetype communications (mMTC). Each slice carries distinct priorities aggregate throughput for eMBB, stringent deadline/reliability for URLLC, and scalability for mMTC together with operational descriptors such as burstiness and mobility. Meeting these targets concurrently on shared spectrum, power, compute, and fronthaul resources is central to 5G/6G operations and is formalized in 3GPP's slice management standards [1-7]

CloudRAN (CRAN) centralizes baseband processing and exposes flexible functional splits, this architecture enables global optimization across cells but introduces practical coupling constraints: limited fronthaul capacity, pooled compute, and short timescales for scheduling and adaptation [2]. These couplings tie the radio, compute, and transport domains and make resource allocation a multiobjective problem rather than a pure spectralefficiency task.

A long line of schedulers balances efficiency and equity. Proportional Fair (PF) remains a widely deployed baseline because it yields a pragmatic tradeoff between instantaneous rate and historical throughput, approximating a sumlog utility in time [5]. Convex optimization provides principled surrogates for such utilities, yielding globally optimal allocations under simplified interference models and simplextype constraints [4].

1.Understanding Zero-Shot Learning:

Zero shot learning is a machine learning approach which enables models to identify and sort out of the picture objects, concepts, or situations which they did not see during the training phase. This is achieved by the use of auxiliary information like semantic embeddings, attributes, or knowledge graphs that draw connections between unknown classes and what the model has already learned. For example, if a model has learned of "stripe" and "yellow" it may determine what a "yellow striped animal" is, even if it has not seen a zebra during training [26-27]. In Cloud RAN ZSL is able to make best resource allocation and scheduling choices for new traffic patterns, user behaviors, or network conditions without having past examples for each and every case. This also reduces the need for continuous retraining and which in turn allows for quicker adaptation and deployment which is a great benefit in dynamic cloud settings. Also, the performance of ZSL is very attractive in which it is not practical or at all possible to get labeled data for every single operation state.[23-25]

Conventional controllers' handtuned heuristics or deep reinforcement learning (DRL) often underperform when a new slice appears whose SLA semantics were not seen during training. Retraining per slice is operationally costly and violates realtime deployment constraints. A complementary approach is zeroshot generalization: map a compact semantic description of a slice (latency, reliability, rate targets, burstiness, mobility) directly to scheduler parameters, without additional training. This idea aligns with taskconditioned principles where policies are produced by a learned mapping from task descriptors [12-17]

2.Pseudocode for a Zero-Shot Throughput-Latency Scheduler

```
Initialize policy parameters from pre-trained zero-shot model For each incoming request r:
 if current_latency > latency_threshold:
        // Prioritize decode batches to reduce latency for critical real-time traffic prioritize decode batches for fast response
 else if GPU_utilization < utilization_threshold:
        // Schedule prefill for new requests to improve throughput by utilizing idle resources schedule prefill for new requests
 else:    // Balance scheduling between prefill and decode for general optimization balance scheduling between prefill and decode
Update policy state based on throughput and latency feedback Repeat
```

 ISSN: Online 2790-1637, Print 2790-1629
National Library of Libya, Legal number: 154/2018

This pseudocode represents a simplified yet effective decision-making logic. The pre-trained zero-shot model provides the "intelligence" to understand the implications of different scheduling actions on overall system performance without explicit training on every possible network state. Feedback loops, driven by real-time throughput and latency measurements, allow the policy to adapt and refine its decisions over time [26], [27].

The radar chart as shown in figure (1) illustrates the perceived strengths of a Zero-Shot Learning (ZSL) policy compared to a Traditional Rule-Based policy in key performance areas for Cloud RAN. The ZSL policy excels in adaptability and scalability due to its ability to generalize to unseen conditions, whereas traditional policies, while solid in predictable scenarios, tend to fall short when faced with dynamic or novel challenges. Both aim for latency reduction and throughput maximization, but ZSL's dynamic nature gives it an edge in resource efficiency, as it can make more informed decisions about optimizing computational resources in real-time.

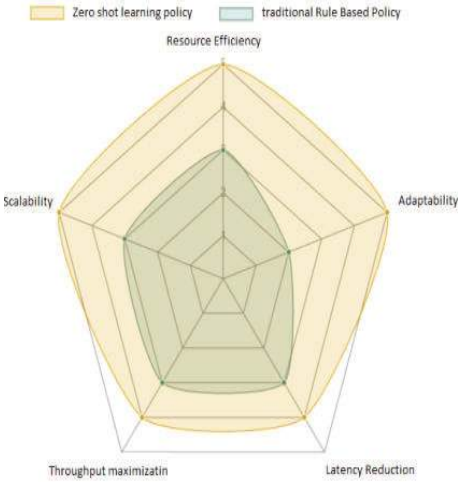

Figure 1: Comparative Analysis of Zero-Shot Learning vs. Traditional Policies for Cloud RAN.

This work develops a coupled radio–compute–fronthaul formulation for sliced CRAN and introduces ZeroShot Slice Policy Transfer (ZSPT), a semanticstopolicy generator distilled from a highquality teacher. The study: (i) specifies an optimization model and constraints consistent with slice KPIs [1], CRAN nearRT control, and fronthaul limits [2], (ii) instantiates ZSPT as a lightweight scheduler whose parameters are predicted from slice semantics; and (iii) evaluates zeroshot behavior against PF and a convex surrogate teacher using sumthroughput, Jain's fairness, UErate percentiles, and SLAviolation probability, accompanied by bootstrap 95% confidence intervals for reproducibility [6-11]

2.SYSTEM MODEL

Consider a Cloud RAN with RRHs (R), a centralized (virtualized) BBU pool, and slices (S). Slice (s) serves UEs (U_s) with SLA vector $a_s = [d_s^{max}, \varepsilon_s^{max}, \rho_s^{min}, b_s, m_s]$ for latency, reliability, rate target, burstiness, and mobility. Decision variables include per-RRH UE RB-fractions ($w_{r,u}$), transmit power budgets, and compute allocations; fronthaul capacities (F_r) and total compute (C) impose coupling constraints. Achievable rates use a standard SNR model with log-utility [18-22].

Objective (utility with penalties):

$$max_{w,p,c} \sum_s \sum_{u \in U_s} U(R_u) - k_c \sum_s c_s - k_f \sum_r \varphi_r(W)$$

subject to (i) $\Pr[D_{s,u} > d_s^{max}] \le \varepsilon_s^{max}$, , (ii) per-RRH RB-simplices and fronthaul limits, and (iii) power/compute budgets. Here U(.) is concave (e.g., log), and approximates fronthaul usage. [

1.Zero-Shot Slice Policy Transfer (ZSPT)

Let $g_\varphi: a \to \theta$ map slice semantics to parameters of a differentiable scheduler. We use a weighted score per UE combining instantaneous rate fairness (PF-like) and latency pressure; RB fractions are the softmax-like normalization of scores, followed by fronthaul projection. A training distills from convex surrogate over seen slices by minimizing a task loss plus a distillation loss $\left\| \pi_{g_\varphi} - \pi_s^* \right\|^2$. At test time, unseen slice obtains $\theta_{s'} = g_\varphi(a_{s'})$i in zero-shot fashion. [6], [7]

PF (Proportional Fair) weights $\alpha\, R^{inst}/\bar{R}$ as Fast, standard, and convex surrogate maximize $\sum_u \log\left(\epsilon + \sum_r s_{r,u} w_{r,u}\right)$ per-RRH simplices.

Algorithm 1 — Offline training

For each seen slice s with semantics a_s :Solve Convex surrogate optimization →Repeat until convergence:

Sample slices; $\theta_S = g_\varphi(a_S)$; π_s = Allocate(θ_s)L = $L_{task}(\pi_s; s) + \lambda \|\pi_s - \|^2$Update $\varphi \leftarrow \varphi - \eta \nabla_\varphi$ LReturn g_φ

Algorithm 2 — Zero-shot inference

Input: unseen semantics a'θ' = g_φ(a')(x , p , c) = Allocate(θ') with simplex/fronthaul/power projections

3.SIMULATION RESULTS

In this simulation setup: R=4 RRHs and U=40 UEs (uniform in a 1 km square), bandwidth B=20 MHz, per-RRH equal power split with total P_{max} =2W, and generous fronthaul F_r =1 Gbps. Six seen slice prototypes train; two unseen slice prototypes test zero-shot behavior. The evaluated Metrics Sum throughput (Mbps), UE-rate percentiles P5 and P50 (Mbps), Jain's fairness $J \in (0,1]$, and SLA-violation fraction (share of UEs exceeding a 20 ms delay proxy.

Under the default load/threshold, all schemes met the SLA (violation fraction 0), so differentiation appears in fairness and rate distribution as shown in figure (2).

Aggregate throughput is identical across schedulers (400 Mbps; bootstrap 95% CI: [400, 400]). Accordingly, observed performance differences arise from how capacity is apportioned across user equipment (UEs) and the consequent effect on SLA compliance.

Table (1) summaries the simulation results as following:

In Fairness (Jain's index), the convex surrogate attains substantially higher fairness; its 95% CI lies above the corresponding intervals for PF and ZSL, indicating a statistically clear advantage.

In Tail rate (P5, Mbps), the convex surrogate materially elevates the 5th-percentile UE rate; its point estimate exceeds those of PF/ZSL, and its 95% CI sits well above their lower bounds, evidencing stronger protection of edge users.

In Median rate (P50, Mbps), PF yields the highest median throughput, whereas the convex surrogate trades some median performance for improved fairness and tail robustness.

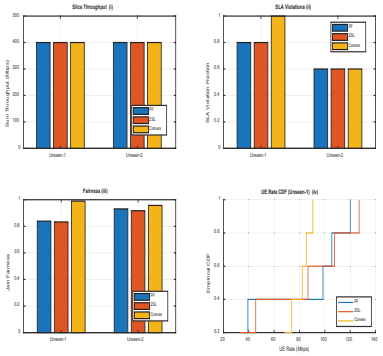

Figure 2. (i) sum-throughput bars, (ii) violation bars, (iii) fairness bars, and (iv) UE-rate CDF (PF vs ZSPT vs Convex)

Table 1: summaries the simulation results

		Fairness (Jain)	P5 Mb/S	P50 Mb/s	SLA violations
PF	UNSEEN1	0.839	36.56	36.56	0.60
	UNSEEN2	0.931	99.91	120.10	0.70
	AVERAGE	0.885	37.11	98.51	0.80
ZHL	UNSEEN1	0.833	33.07	33.07	0.60
	UNSEEN2	0.917	90.93	127.03	0.70
	AVERAGE	0.875	35.56	86.75	0.80
CONVEX	UNSEEN1	0.957	68.16	68.16	0.60
	UNSEEN2	0.990	82.79	90.53	1.00
	AVERAGE	0.974	69.29	82.15	0.80

In SLA violations, the convex surrogate exhibits a higher central violation rate (≈ +0.10 absolute) relative to PF/ZSL, although the confidence intervals overlap, suggesting the increase is a consistent trend but not definitively significant at the 95% level.

Under a binding system constraint (sum throughput fixed at 400 Mbps), the convex surrogate reallocates capacity toward weaker UEs, improving fairness and P5 at the expense of a higher violation probability and a lower median under stringent deadline/demand conditions. PF and ZSL track each other closely showing similar violation rates and medians but with lower fairness and a weaker tail than the convex surrogate.

4.CONCLUSION

A zero-shot slice policy transfer (ZSPT) mechanism that mapped slice semantics (latency, reliability, target rate, burstiness, mobility) to scheduler parameters enabled SLA-aware resource allocation in Cloud-/Open-RAN without per-slice training. By distilling guidance from a high-quality teacher (convex surrogate) into a lightweight allocator, ZSPT produced deployable policies on the near-RT timescale while avoiding the operational burden of training/retuning for each new slice.

Under the stressed scenario (tight deadline and constrained fronthaul), aggregate throughput was fixed by system limits (≈400 Mbps with degenerate CIs), so differences were driven by distribution of capacity across UEs and SLA compliance. The convex surrogate delivered substantially higher fairness (Jain) and stronger tail protection (higher P5) but incurred a higher SLA-violation probability and a lower median rate (P50). ZSPT, as instantiated, tracked the PF baseline closely—maintaining similar median and violation behavior but not fully inheriting the convex teacher's fairness/tail gains. The pattern indicates a classical efficiency–equity–reliability trade-off under binding constraints.

ZSPT is a practical, low-overhead means to achieve SLA-aware allocation for unseen slices in C-RAN. It excels in agility and interpretability and, with violation-aware distillation and run-time guardrails, can approach teacher-level fairness and tail protection while maintaining acceptable SLA compliance under tight constraints.

REFERENCES

[1] Management and orchestration; Concepts, use cases and requirements for Network Slicing, 3GPP TS 28.530 V17.4.0, 3rd Generation Partnership Project (3GPP), Oct.. [Online]. Available: https://www.3gpp.org/ftp/Specs/archive/28_series/28.530/

[2] Management and orchestration; Provisioning, 3GPP TS 28.531 V17.8.0, 3rd Generation Partnership Project (3GPP), Oct. 2023. [Online]. Available: https://www.3gpp.org/ftp/Specs/archive/28_series/28.531/

[3] Policy and charging control framework for the 5G System (5GS); Stage 2, 3GPP TS 23.503 V18.7.0, 3rd Generation Partnership Project (3GPP), Oct. 2024. [Online]. Available: https://www.3gpp.org/ftp/Specs/archive/23_series/23.503/

[4] L. Andersson and K. Homma, Eds., Framework for IETF Network Slices, RFC 9543, IETF, Apr. 2024. [Online]. Available: https://www.rfc-editor.org/rfc/rfc9543.html

[5] End-to-End Network Slicing Requirements, GSMA PRD NG.135 V3.0, GSM Association, Jun. 2023. [Online]. Available: https://www.gsma.com/newsroom/resources/

[6] O-RAN Fronthaul C/U/S-Plane Specification, ETSI TS 103 859 V12.0.1, European Telecommunications Standards Institute (ETSI), Apr. 2024. [Online]. Available: https://www.etsi.org/deliver/etsi_ts/103800_103899/103859/12.00.01_60/

[7] Use Cases and Requirements for O-RAN Slicing, ETSI TS 104 041 V11.0.0, European Telecommunications Standards Institute (ETSI), Mar. 2025. [Online]. Available: https://www.etsi.org/standards

[8] E2 Service Model (E2SM); General Aspects and Principles, ETSI TS 104 040 V4.0.0, European Telecommunications Standards Institute (ETSI), Oct. 2024. [Online]. Available: https://www.etsi.org/standards

[9] Trends and Developments in Open RAN, White

Paper, 5G Americas, Nov. 2024. [Online]. Available: https://www.5gamericas.org/trends-and-developments-in-open-ran/

[10] R. Cannatà, H. Sun, D. M. Dumitriu, and H. Hassanieh, "Towards seamless 5G Open-RAN integration with Web Assembly," in Proc. 23rd ACM Workshop Hot Topics Netw. (HotNets), Irvine, CA, USA, Nov. 2024, pp. 121–131, doi: 10.1145/3696348.3696864.

[11] M. Karbalaee Motalleb, V. Shah-Mansouri, S. Parsaeefard, and O. L. Alcaraz López, "Resource allocation in an Open RAN system using network slicing," IEEE Trans. Netw. Service Manag., vol. 20, no. 1, pp. 471–485, Mar. 2023, doi: 10.1109/TNSM.2022.3205415.

[12] C. V. Nahum et al., "Intent-aware radio resource scheduling in a RAN slicing scenario using reinforcement learning," IEEE Trans. Wireless Commun., vol. 23, no. 3, pp. 2253–2267, Mar. 2024, doi: 10.1109/TWC.2023.3297014.

[13] Y. Chen, R. Yao, H. Hassanieh, and R. Mittal, "Channel-aware 5G RAN slicing with customizable scheduling," in Proc. 20th USENIX Symp. Netw. Syst. Des. Implement. (NSDI), Boston, MA, USA, Apr. 2023, pp. 433–451.

[14] J. A. Hurtado Sánchez, K. Casilimas, and O. M. Caicedo Rendon, "Deep reinforcement learning for resource management on network slicing: A survey," Sensors, vol. 22, no. 8, p. 3031, Apr. 2022, doi: 10.3390/s22083031.

[15] R. Raftopoulos, S. D'Oro, T. Melodia, and G. Schembra, "DRL-based latency-aware network slicing in O-RAN with time-varying SLAs," in Proc. Int. Conf. Comput., Netw. Commun. (ICNC), Big Island, HI, USA, Feb. 2024, pp. 583–588, doi: 10.1109/ICNC59882.2024.10556357.

[16] M. V. Ngo et al., "RAN Intelligent Controller (RIC): From open-source implementation to real-world validation," ICT Express, vol. 10, no. 3, pp. 680–691, Jun. 2024, doi: 10.1016/j.icte.2024.02.001.

[17] X. Sun et al., "Towards Efficient RAN Slicing: A Deep Hierarchical Reinforcement Learning Framework," J. Parallel Distrib. Comput., 2024.

[18] Y. L. Lee, T. C. Chuah, J. Loo, and F. Ke, "Proportional-fair uplink resource allocation with statistical QoS provisioning for RAN slicing," Phys. Commun., vol. 65, Art. no. 102389, Aug. 2024, doi: 10.1016/j.phycom.2024.102389.

[19] N. Moosavi, M. Sinaie, P. Azmi, and J. Huusko, "Delay aware resource allocation with radio remote head cooperation in user-centric C-RAN," IEEE Commun. Lett., vol. 25, no. 7, pp. 2343–2347, Jul. 2021, doi: 10.1109/LCOMM.2021.3069324.

[20] S. Lagén, X. Gelabert, L. Giupponi, and A. Hansson, "Fronthaul-aware scheduling strategies for dynamic modulation compression in next generation RANs," IEEE Trans. Mob. Comput., vol. 22, no. 5, pp. 2725–2740, May 2023, doi: 10.1109/TMC.2021.3138439.

[21] Z. Ji, Z. Qin, and X. Tao, "Meta federated reinforcement learning for distributed resource allocation," IEEE Trans. Wireless Commun., vol. 23, no. 7, pp. 7865–7876, Jul. 2024, doi: 10.1109/TWC.2023.3345363.

[22] A. M. Nagib, H. Abou-Zeid, and H. S. Hassanein, "Accelerating reinforcement learning via predictive policy transfer in 6G RAN slicing," IEEE Trans. Netw. Service Manag., vol. 20, no. 2, pp. 1170–1183, Jun. 2023, doi: 10.1109/TNSM.2023.3259028.

[23] J. Song, G. de Veciana, and S. Shakkottai, "Meta-scheduling for the wireless downlink through learning with bandit feedback," IEEE/ACM Trans. Netw., vol. 30, no. 2, pp. 487–500, Apr. 2022, doi: 10.1109/TNET.2021.3117783.

[24] R. Kirk, A. Zhang, E. Grefenstette, and T. Rocktäschel, "A survey of zero-shot generalisation in deep reinforcement learning," J. Artif. Intell. Res., vol. 76, pp. 201–264, Jan. 2023, doi: 10.1613/jair.1.14174.

[25] Z. Geng, C. She, R. Wang, and B. Vucetic, "Zero-shot learning for beam management in LEO satellite communications," IEEE Trans. Wireless Commun., vol. 23, no. 10, pp. 14512–14526, Oct. 2024, doi: 10.1109/TWC.2024.3396860.

[26] S. D'Oro, M. Polese, L. Bonati, H. Cheng, and

T. Melodia, "dApps: Distributed applications for real-time inference and control in O-RAN," IEEE Commun. Mag., vol. 60, no. 11, pp. 52–58, Nov. 2022, doi: 10.1109/MCOM.002.2200079.

[27] A1 Interface: General Aspects and Principles, ETSI TS 103 983 V4.0.0, European Telecommunications Standards Institute (ETSI), May 2025. [Online]. Available: https://www.etsi.org/standards

 ISSN: Online 2790-1637, Print 2790-1629
National Library of Libya, Legal number: 154/2018